

## A CHANDRA SURVEY OF THE NEAREST ULIRGS: OBSCURED AGN OR SUPER-STARBURSTS?

A. PTAK, T. HECKMAN AND D. STRICKLAND<sup>2</sup>

The Johns Hopkins University, Dept. of Physics and Astronomy, Baltimore, MD 21218

N. A. LEVENSON

Department of Physics and Astronomy, University of Kentucky, Lexington, KY 40506

K. WEAVER<sup>1</sup>

NASA Goddard Space Flight Center, Laboratory for High Energy Astrophysics

(Received 2002 October 1)  
*Accepted for August 2003 ApJ*

### ABSTRACT

We present initial results from a Chandra survey of a complete sample of the 8 nearest ( $z \leq 0.04$ ) ultraluminous IR galaxies (ULIRGs), and also include the IR-luminous galaxy NGC 6240 for comparison. In this paper we use the hard X-rays (2-8 keV) to search for the possible presence of an obscured AGN. In every case, a hard X-ray source is detected in the nuclear region. If we divide the sample according to the optical/IR spectroscopic classification (starburst *vs.* AGN), we find that the 5 “starburst” ULIRGs have hard X-ray luminosities about an order-of-magnitude smaller than the 3 “AGN” ULIRGs. NGC 6240 has an anomalously high hard X-ray luminosity compared to the “starburst” ULIRGs. The Fe K $\alpha$  line is convincingly detected in only two ULIRGs. The weakness of the Fe-K emission in these ULIRGs generally suggests that the hard X-ray spectrum is not dominated by reflection from high  $N_H$  neutral material. The hard X-ray continuum flux ranges from a few  $\times 10^{-3}$  to a few  $\times 10^{-5}$  of the far-IR flux, similar to values in pure starbursts, and several orders-of-magnitude smaller than in Compton-thin AGN. The upper limits on the ratio of the Fe K $\alpha$  to far-IR flux are below the values measured in Compton-thick type 2 Seyfert galaxies. While very large column densities of molecular gas are observed in the nuclei of these galaxies, we find no evidence that the observed X-ray sources are obscured by Compton-thick material. Thus, our new hard X-ray data do not provide direct evidence that powerful “buried quasars” dominate the overall energetics of most ultraluminous infrared galaxies.

*Subject headings:* evolution-galaxies:evolution–X-rays: galaxies–X-rays

### 1. INTRODUCTION

Ultraluminous IR galaxies (ULIRGs) are defined to be galaxies whose bolometric luminosity exceeds  $10^{12}L_{\odot}$  and whose emission is dominated by the mid- and far-infrared bands (Sanders & Mirabel 1996).<sup>3</sup> They are thought to be powered by either an AGN (Sanders 1999), a very powerful nuclear starburst (Joseph 1999), or both. It is possible that these galaxies are an evolutionary stage of normal galaxies in which a large amount of dense gas that has been driven to the nucleus is both feeding a nuclear black hole and fueling a very high star-formation rate (Norman & Scoville 1988).

ULIRGs generically have highly disturbed morphologies suggestive of severe tidal effects, and often have double nuclei suggestive of the late stages of a galaxy merger (Clements, Sutherland, McMahon, & Saunders 1996). If elliptical galaxies are the by-product of similar mergers, then ULIRGs should have been very common in the early universe (Genzel et al. 2001). This is consistent with the properties of the sub-mm source population, and the corresponding estimates for the star-formation history of the universe (Blain et al. 1999).

ULIRGs offer ideal local laboratories for studying the processes occurring in the high-redshift sub-mm sources.

As such, decoupling the effects of an AGN and star-formation is important for assessing the role of ULIRG-like objects in building present-day elliptical galaxies, in accounting for the total amount of energy supplied by AGN over cosmic time, and in establishing the strong correlation between the mass of a supermassive black hole and the properties of its “host” galaxy spheroid (Ferrarese & Merritt 2000; Tremaine et al. 2002).

The nature of the central power-source in ULIRGs remains uncertain, owing to its location behind large column densities of obscuring material. This highlights the importance of observations in the hard X-ray, far-IR, and radio domain, which most effectively pierce the obscuring material. However, such observations to date have not provided decisive evidence to break the AGN/starburst deadlock (because they have lacked either the appropriate spatial resolution or have not provided unambiguous spectroscopic discriminants between AGN and starbursts).

The optical and near/mid-IR regimes contain many potentially important spectral diagnostics. Such observations of ULIRGs variously classify them as Seyferts, LINERs or starbursts (Genzel et al. 1998; Imanishi & Dudley 2000; Kewley, Heisler, Dopita, & Lumsden 2001; Kim, Veilleux, & Sanders 1998; Laurent et al.

<sup>3</sup> We assume  $H_0 = 70 \text{ km s}^{-1} \text{ Mpc}^{-1}$ .

2000; Veilleux, Kim, Sanders, Mazzarella, & Soifer 1995; Veilleux, Kim, & Sanders 1999; Veilleux, Sanders, & Kim 1999). If the ULIRGs optically classified as LINERs are considered to be starburst-driven, then there is good overall agreement between the optical and IR classifications (Lutz, Veilleux, & Genzel 1999; Taniguchi, Yoshino, Ohyama, & Nishiura 1999), and in general nearby LINERs exhibiting only narrow H $\alpha$  lines tend to have X-ray properties more consistent with a starburst rather than an AGN interpretation (Eracleous et al. 2002; Terashima, Ho, & Ptak 2000). However, X-ray observations of the infrared-luminous merger NGC 6240 (which appears to be starburst-dominated LINER from an optical/IR perspective) reveal a powerful AGN that may dominate its energetics (Vignati et al. 1999).

Observations of ULIRGs with the Chandra X-ray Observatory promise to be enlightening for this issue. Chandra has large effective area, high spatial resolution (FWHM  $\sim 1''$ ), and is capable of moderate spectral resolution imaging spectroscopy. All of these may be necessary to determine the physical origin of the hard X-ray emission previously detected from ULIRGs (Risaliti, Gilli, Maiolino, & Salvati 2000). Recently, Gallagher et al. (2002), Xia et al. (2002), and Clements et al. (2002) have presented detailed analysis of Chandra observations of the ULIRGs Mkn 231, Mkn 273, and Arp 220 respectively (see also McDowell et al. 2003). Our approach here is to examine a sample of ULIRGs that is large enough to document the properties of the class as-a-whole.

The eight ULIRGs listed in Table 1 comprise both a flux-limited sample with  $F_{60\mu} > 10$  Jy, and a volume-limited sample out to  $cz = 14000$  km s $^{-1}$  ( $D < 200$  Mpc), and NGC 6240 is included since it is an archetype of IR-luminous galaxies shown by hard X-ray data to harbor a powerful AGN (Iwasawa & Comastri 1998). Note that the galaxies are all at a redshift of  $\sim 0.04$  with the exceptions of Arp 220 and NGC 6240 ( $z \sim 0.02$ ). The joint analysis of XMM-Newton and Chandra data for two of these galaxies (IRAS 05189-2524 and UGC 05101) will be presented in future work. An analysis of the spatially-resolved soft X-ray emission and a comparison to models of galactic winds will also be presented elsewhere.

The organization of the present paper is as follows. In section 2 we describe the data reduction and analysis techniques. In section 3 we discuss the results of spatial and spectral fitting of the data. In section 4 we discuss the implications of these results.

## 2. DATA REDUCTION

The observation dates and net exposure times for our targets are listed in Table 1. The data for Arp 220, Mkn 231, Mkn 273 and NGC 6240 were downloaded from the Chandra archive. The data reduction was performed using CIAO 2.2 and the data were reprocessed using CALDB 2.9. XAssist (see Ptak & Griffiths 2002), which is a software package that assists in data reprocessing, initial source selection and analysis, was also used in the analysis of these data. Briefly, XAssist performs the basic data reduction steps recommended by the CXC “threads” (note that the 0.5 pixel position randomization is also removed, which is an optional step). Sources are detected using wavdetect, the background

light curve is examined and time of background flaring are removed, and the image of each source is fitted with an elliptical gaussian model in order to determine the spatial extent (see section 3). The data were analyzed in full (0.3-8.0 keV), soft (0.5-2.0 keV) and hard (2.0-8.0 keV) bandpasses. For comparison with previous X-ray studies a region was selected (manually) that encompassed the entire X-ray extent of the galaxy (determined from the full-band images) and spectra were extracted for these “global” regions. The spectra were binned to 20 counts/channel to allow use of the  $\chi^2$  statistic.

Figure 1 shows adaptively-smoothed soft and hard band images, with the global and nuclear regions marked. We show the soft band images here for completeness, but defer their analysis. Note that the nuclear regions were chosen to maximize the signal-to-noise of the nuclear spectrum while the emphasis for the global regions was complete coverage of the X-ray emission of the galaxies (in part for comparison with previous X-ray studies). We checked for counterparts to all X-ray sources within the central 8' of the observation (where the PSF size is  $< 1''$ ) using HEASARC databases containing stars (USNO and GSC2.2), QSOs, 2Mass sources and the FIRST survey. In general, only a few counterparts in each field were found. These show that the astrometric solutions are good to  $\sim 0.5 - 1''$ , but could not be used to apply reliable astrometric corrections.

## 3. SPATIAL ANALYSIS

### 3.1. Nuclear Source Sizes

The extents derived from the spatial fitting procedure are listed in Table 2. The fitting was performed using the C fit statistic (Cash 1979) and the errors correspond to  $\Delta C = 4.605$  (90% confidence interval for 2 interesting parameters). In all but three cases, the nuclear 2.0-8.0 keV source is consistent with being unresolved (FWHM  $\lesssim 1''$ ). The hard X-ray emission in the nuclei of both IRAS 17208-0014 and Arp 220 are resolved and asymmetric, with a major axis FWHM of 2.6'' (0.9 kpc) in Arp 220 and 4.7'' (3.9 kpc) in IRAS 17208-0014. Point sources are present in the FOV with Gaussian fit FWHM parameters of  $\sim 1''$ , indicating that the elongation in IRAS 17208-0014 is not due to errors in the aspect solution. In NGC 6240, the hard X-ray nuclear emission is resolved into two sources coincident with the radio nuclei, and diffuse emission, consistent with the full-band HRC results reported in Lira, Ward, Zezas & Murray (2002) and the ACIS results reported in Komossa et al. (2003). However for consistency with the rest of the sample we model the hard X-ray flux with a single Gaussian to determine the extent of the total (i.e., combined) nuclear flux, noting that the individual nuclei would not have been resolved at redshifts  $\gtrsim 0.04$  (see also below).

In order to further investigate the presence of unresolved hard X-ray emission the 2-8 keV nuclear emission was fit with a Gaussian model convolved with a PSF image generated using the CIAO tool mkpsf (using a photon energy of 3 keV, where the 2-8 keV photon spectrum generally peaks for these sources). For the galaxies with a nuclear point source, the main impact of including the PSF was to reduce the source extent parameter  $\sigma$  from  $\sim 0.5''$  to  $\sim 0.25''$ : that is, the model PSF convolved with a Gaussian with  $\sigma=0.25''$  (FWHM = 0.6 arcsec) provides

TABLE 1. BASIC DATA FOR THE ULIRG SAMPLE.

| Galaxy         | Position<br>(J2000)  | z      | Scale<br>(kpc/'') | Date                     | Exposure<br>(ks) | Galactic $N_H$<br>( $10^{20} \text{ cm}^{-2}$ ) |
|----------------|----------------------|--------|-------------------|--------------------------|------------------|---|
| IRAS05189-2524 | 05 21 01.5 -25 21 45 | 0.0426 | 0.82              | 10/30/2001<br>01/30/2002 | 6.6<br>14.8      | 4   |
| UGC 05101      | 09 35 51.6 +61 21 11 | 0.0394 | 0.76              | 05/28/2001               | 49.3             | 3   |
| Mkn 231        | 12 56 14.2 +56 52 25 | 0.0422 | 0.82              | 10/19/2000               | 34.5             | 1   |
| Mkn 273        | 13 44 42.1 +55 53 13 | 0.0378 | 0.74              | 04/19/2000               | 44.2             | 1   |
| Arp 220        | 15 34 57.1 +23 30 11 | 0.0181 | 0.36              | 06/24/2000               | 56.4             | 4   |
| NGC 6240       | 16 52 58.9 +02 24 03 | 0.0245 | 0.49              | 07/29/2001               | 36.6             | 6   |
| IRAS17208-0014 | 17 23 21.9 -00 17 00 | 0.0428 | 0.83              | 10/24/2001               | 48.5             | 10  |
| IRAS20551-4250 | 20 58 26.9 -42 39 0  | 0.0428 | 0.83              | 10/31/2001               | 40.4             | 4   |
| IRAS23128-5919 | 23 15 47.0 -59 03 17 | 0.0446 | 0.86              | 09/30/2001               | 33.8             | 3   |

NOTE. — Positions and redshifts were obtained from NED. Galactic  $N_H$  values are determined from Dickey & Lockman (1990) using the LHEASOFT tool “nh” (<http://heasarc.gsfc.nasa.gov>)

TABLE 2. NUCLEAR SPATIAL PROPERTIES

| Galaxy          | Soft Emission    |                  |               | Hard Emission    |                  |                 |
|-----------------|------------------|------------------|---------------|------------------|------------------|-----------------|
|                 | $\sigma_x$ (")   | $\sigma_y$ (")   | $\theta$      | $\sigma_x$ (")   | $\sigma_y$ (")   | $\theta$        |
| Arp 220         | 1.05 (1.03-1.06) | 0.97 (0.95-0.98) | 64 (59-67)    | 0.99 (0.86-1.14) | 0.68 (0.57-0.82) | 190 (175 - 210) |
| IRAS05189-2524  | 0.46 (0.42-0.49) | = $\sigma_x$     | ...           | 0.44 (0.41-0.47) | = $\sigma_x$     | ...             |
| IRAS05189-2524* | 0.50 (0.46-0.53) | = $\sigma_x$     | ...           | 0.46 (0.44-0.48) | = $\sigma_x$     | ...             |
| IRAS17208-0014  | 2.02 (1.62-2.53) | 1.45 (1.20-1.76) | 57 (34-81)    | 1.05 (0.89-1.26) | 0.58 (0.48-0.74) | 66 (54-81)      |
| IRAS20551-4250  | 1.53 (1.15-1.86) | 1.06 (0.76-1.33) | 150 (127-170) | 0.65 (0.53-0.84) | = $\sigma_x$     | ...             |
| IRAS23128-5919  | 1.35 (0.94-1.70) | 0.77 (0.55-1.06) | 146 (131-168) | 0.43 (0.38-0.48) | = $\sigma_x$     | ...             |
| Mkn 231         | 0.43 (0.40-46)   | = $\sigma_x$     | ...           | 0.42 (0.40-0.44) | = $\sigma_x$     | ...             |
| Mkn 273         | 1.17 (1.06-1.29) | 0.61 (0.53-0.69) | 45 (38-52)    | 0.59 (0.55-0.64) | 0.47 (0.43-0.50) | 141 (128-152)   |
| NGC 6240        | 1.85 (1.72-1.99) | 2.79 (2.58-3.04) | 158 (150-166) | 0.80 (0.72-0.88) | 1.19 (1.12-1.26) | 14.5 (8.9-21.4) |
| UGC 05101       | 0.97 (0.83-1.10) | = $\sigma_x$     | ...           | 0.55 (0.46-0.63) | = $\sigma_x$     | ...             |

NOTE. — Fit results based on fitting an elliptical gaussian model where surface brightness =  $N e^{-[(\frac{x}{2\sigma_x})^2 + (\frac{y}{2\sigma_y})^2]}$ , and x, y are rotated from the right ascension axis by  $\theta$  (given in degrees). Note that these fits were performed only to the nuclear source in images extracted from the central  $5''$  of these galaxies, and as shown in Figure 1 often emission is present on larger spatial scales.

\*2nd observation of IRAS 05189-2524.

a good fit to the nuclear point sources in these ULIRGs. We regard this as an upper limit to the true source size, since it may arise from errors in the aspect solution.

As stated above, NGC 6240 is resolved into two faint sources in addition to diffuse flux. Modeling this flux as a combination of two point sources in addition to two elliptical Gaussians (to account for diffuse flux associate with each nuclei) we find that the northern and southern nuclei contribute 17% and 28% of the 2-8 keV counts from the central  $9''$  ( $\sim 0.5$  kpc) of NGC 6240. In the cases of Arp 220 and IRAS 17208-0014, the diffuse emission was modeled with elliptical Gaussians and the PSF  $\times$  Gaussian model with  $\sigma = 0.25''$  was placed at the centroid of the diffuse flux. This resulted in upper limits (for  $\Delta C = 4.605$ ) of  $1.2 \times 10^{-3}$  and  $4.3 \times 10^{-4}$  counts  $s^{-1}$  for the 2-8 keV count rate of a point source, respectively, or 2-10 keV fluxes of  $4.5 \times 10^{-14}$  erg  $cm^{-2} s^{-1}$  and  $8.3 \times 10^{-15}$  erg  $cm^{-2} s^{-1}$  ( $L_{2-10 \text{ keV}} \sim 4 \times 10^{40}$  erg  $s^{-1}$  in both cases). Finally, we note that in Arp 220 there is a  $\sim 1.7''$  (0.6 kpc) offset between the hard and soft nuclear positions, with the hard nucleus being coincident with the western 6 cm nucleus discussed in Norris (1988) and the soft nucleus being offset to the NW of the hard nucleus (Clements et al. 2002). The soft nucleus is not coincident with either radio nucleus and is most likely

due to hot ISM observed through a region with relatively low extinction. Note that the optical nucleus of Arp 220 is similarly offset by  $\sim 2''$  to the NW of the western radio nucleus, which has likewise been interpreted as the result of a “hole” in the extinction toward the nucleus (Arribas, Colina, & Clements 2001).

### 3.2. Extra-nuclear Point Sources

Table 3 lists the positions and luminosities of unresolved sources that were detected within the X-ray extent of the galaxies. The luminosities were computed assuming a power-law model with a photon index of 1.8. If these sources are associated with the corresponding host galaxy, then they have luminosities well in excess of the Eddington luminosity of a solar-mass black hole or neutron star X-ray binary, and hence are “ultraluminous X-ray objects” (ULXs; also known as intermediate-luminosity X-ray objects or IXOs). Note that the ULX in UGC 05101 has a very hard spectrum (i.e., it is not present in the soft-band image in Figure 1) which may be indicative of a highly-absorbed spectrum with  $N_H > 10^{22-23} \text{ cm}^{-2}$ . Since this source is not in the nucleus of UGC 05101, this would imply a large amount of internal absorption for this source. Gallagher et al. (2002) also discuss an ULX in Mkn 231 which lies below our detection threshold of  $\sim 10$  counts. Finally, the

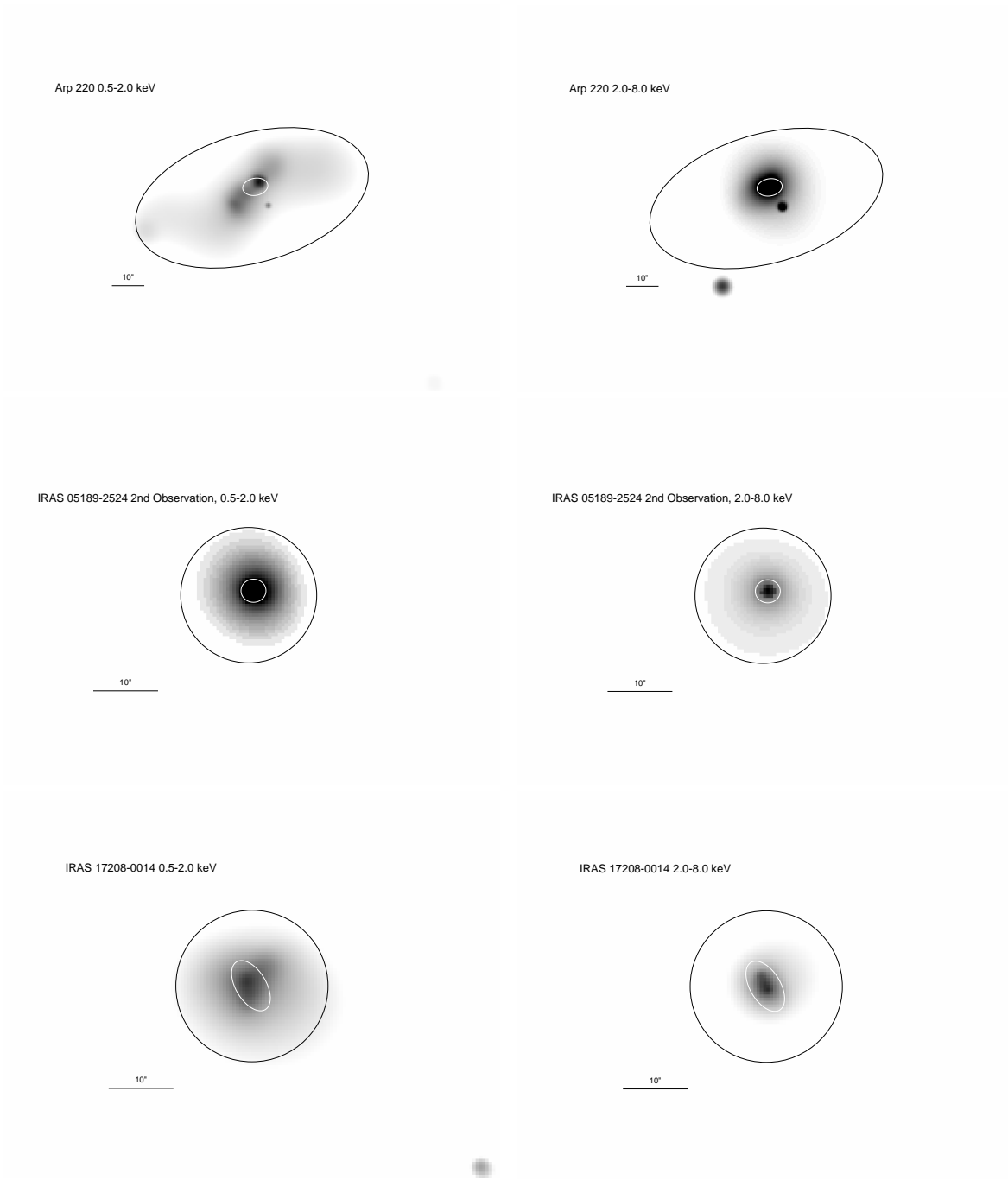


FIG. 1.—

ULX in IRAS 20511-4250 has an estimated hard X-ray luminosity that is  $\sim 20\%$  of the luminosity of the nuclear source in this galaxy. However, this luminosity is highly uncertain given the low count rate of the source. The 2-8 keV count rate of the ULX is  $\sim 25\%$  of global 2-8 keV count rate.

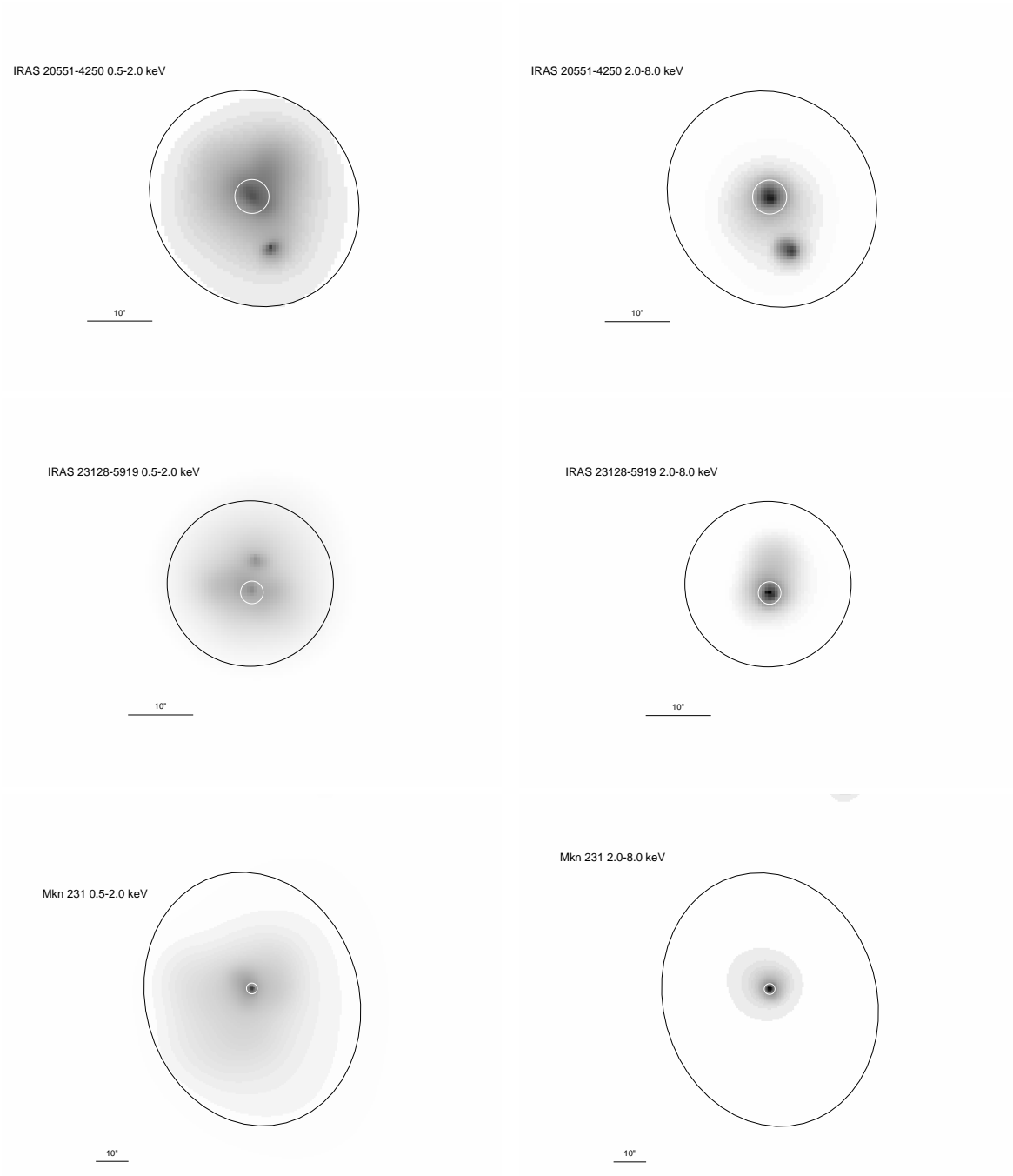


FIG. 1.— (cont.)

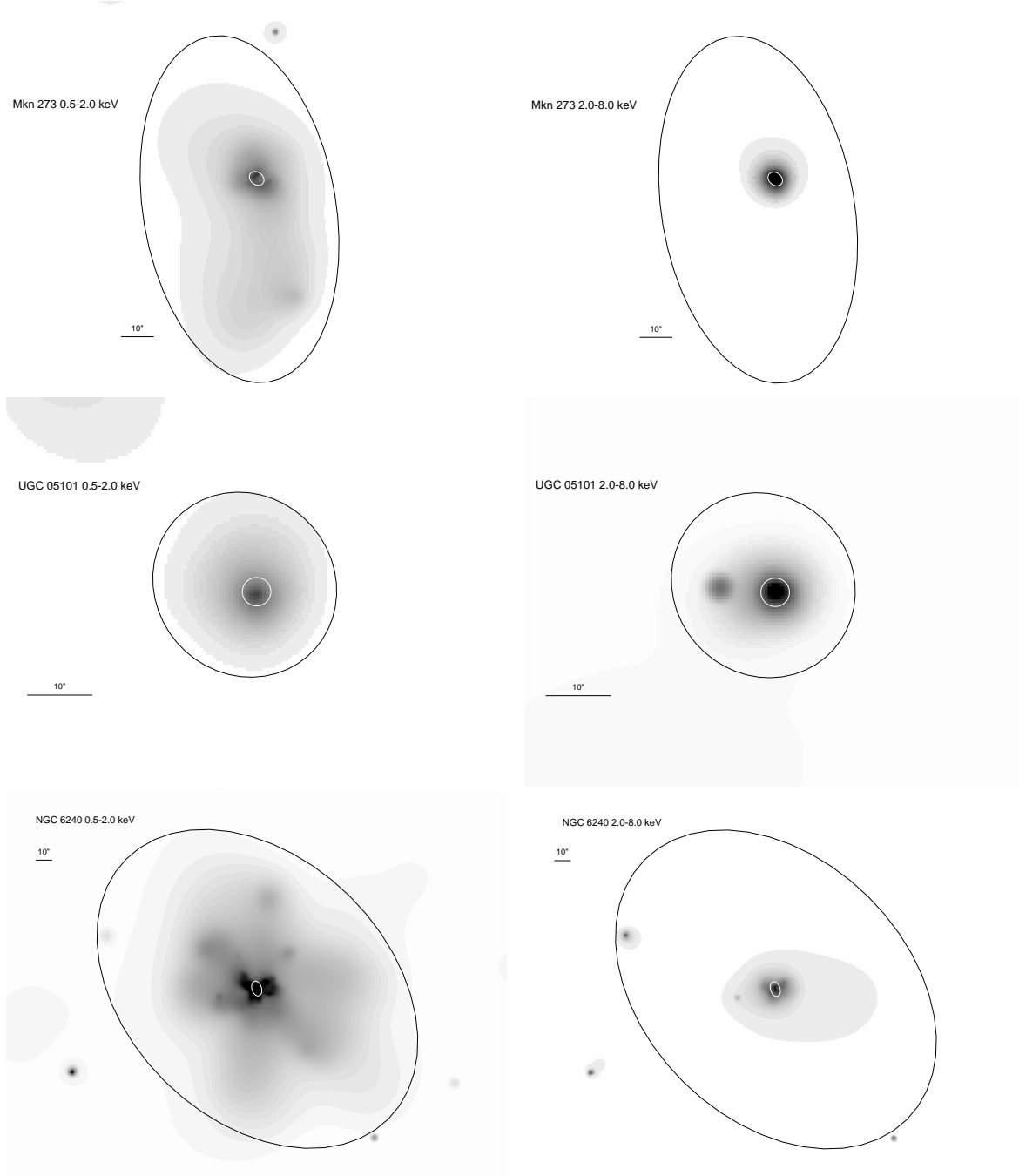


FIG. 1.— (cont.) 0.5-2.0 keV and 2.0-8.0 keV images of the ULIRG sample. The outer and inner ellipses show the global and nuclear source region, respectively. The images were adaptively smoothed to a significance level of  $2.8\sigma$  and scaled logarithmically. N is up and E is to the left in these images.

### 3.3. Large-Scale Emission

In addition to the nuclear source and the extranuclear point sources, extended hard X-ray emission is often detected beyond the nuclear region on scales of  $\sim 10$  kpc. The fraction of total hard X-ray flux in this spatially-extended component is  $\leq 10\%$  in four cases (Arp 220, IRAS 05189-2524, Mkn 273, and Mkn 231), but ranges from 30 to 50% in the other cases (Figure 1). Note that in the case of IRAS 20551-4250, the extra-nuclear unresolved source may account for up to  $\sim 50\%$  of the extra-nuclear hard X-ray flux.

## 4. SPECTRAL ANALYSIS

As stated above, in every galaxy a nuclear core was detected in the 2-8 keV data. We proceeded initially by using XSPEC to fit these spectra with a simple absorbed power-law model. The results of this procedure are given in Table 4. Errors (corresponding to  $\Delta\chi^2 = 4.605$ ) are only derived for fits in which  $\chi^2/\text{dof} < 1.5$ . Figure 2 shows the data and model for these fits. These fits result in  $\chi^2/\text{dof} < 1.5$  only in the cases of IRAS 17208-0014 and Mkn 231.

We next tried to fit each spectrum with a “mekal” plasma (Liedahl, Osterheld, & Goldstein 1995) plus power-law model. In these fits, absorption is applied to the entire spectrum with a hard lower-limit on the column density set to be 50% of the Galactic column, and a second absorber at the redshift of the ULIRG is applied only to the power-law component. Based on X-ray spectroscopy of starburst galaxies, the temperature of the plasma was limited to the range 0.3-2.0 keV. If the temperature was not constrained by the data then it was held fixed at 0.7 keV. Likewise, the abundance was limited to the range of  $Z = 0 - 5Z_\odot$ , and fixed at  $1.0Z_\odot$  if not constrained. The results are given in Table 5 and plotted in Figure 3. Here all fits have  $\chi^2/\text{dof} < 1.5$  except in the cases of Mkn 273, UGC 05101 and NGC 6240 (due to Fe-K emission, see below). Note that this more complex model is statistically preferred to the simple power-law model for Mkn 231. Significant residuals are evident in the case of Arp 220 around 0.8 and 1.8 keV, possibly the result of non-solar O and Si abundances or additional thermal components at different temperatures being required. A degeneracy between these scenarios is often observed in nearby starburst galaxies (e.g., Weaver, Heckman, & Dahlem 2000).

Chandra observations of bright point sources may suffer from pile-up (Davis 2001). This is only a concern for IRAS 05189-2524, the brightest ULIRG in our sample and the only one that is completely unresolved at both soft and hard X-ray energies (see also the pile-up discussion concerning Mkn 231 in Gallagher et al. 2002). We assessed the amount of pile-up by modeling the 2nd observation, which had the higher count rate, using MARX. This analysis indicated that  $\sim 20\%$  of the Chandra counts are piled-up in that observation. We checked the impact by fitting the two spectra from the two observations of IRAS 05189-2524 with the plasma plus power-law model, additionally including the “pile-up” convolution model in XSPEC (based on Davis 2001). We allowed the overall normalization and the pile-up grade migration parameter to vary independently. This resulted in a power-law slope of  $\Gamma = 1.1$ , consistent with the indi-

vidual fits, and showed that we are underestimating the 2-10 keV flux of IRAS 05189-2524 by  $\sim 15\%$ . Therefore pile-up does not affect our conclusions.

### 4.1. Fe-K $\alpha$ Emission

In Mkn 273 and NGC 6240, strong Fe-K emission is present, and Fe-K emission is marginally detected in UGC 05101 (joint analysis of the Chandra and XMM-Newton data, to be presented elsewhere, verifies the existence of the line). In Table 6 we show the results of including a Gaussian line in the plasma + power-law model fits for IRAS 05189-2524, Mkn 231, Mkn 273, NGC 6240, and UGC 05101 (insufficient counts are detected from the other ULIRGs for these fits to result in useful constraints). We also calculate the upper limits for a narrow line (physical width = 0.01 keV; the resolution of ACIS-S at  $\sim 6$  keV is  $\sim 0.1$  keV), and lines with physical widths of 0.1 and 0.5 keV at 6.7 keV using absorbed power-law models applied to the 2-8 keV spectra of IRAS 05189-2524 and Mkn 231. 6.7 keV would correspond to the K $\alpha$  emission from Fe XXV. Such a line would be expected from an ionized scattering region, and we computed the upper limits assuming a non-negligible physical width to demonstrate the impact of a range of ionization states being present. Note that the Fe-K line from IRAS 05189-2524 reported in Severgnini et al. (2001) is not detected in our Chandra (or XMM-Newton) data, although the significance of the line in the prior observations was low and our upper-limits are consistent with the errors.

The hard X-ray continuum is usually very weak, and in many cases the resulting uncertainties on the continuum fit are substantial. Thus, a more direct (model-independent) upper limit to the Fe-K $\alpha$  flux was determined by interpolating the local background plus continuum flux across the region of the Fe-K $\alpha$  line in the spectra, and then setting an upper bound to the excess of line photons. As a consistency check, we computed the flux of the Fe-K line in Mkn 273 directly from the spectrum in this fashion, which resulted in a value of  $4.5 \times 10^{-14}$  erg cm $^{-2}$  s $^{-1}$  which is consistent with the value of  $6.0 \times 10^{-14}$  erg cm $^{-2}$  s $^{-1}$  obtained from the fit listed in Table 6. The resulting upper limits on the K $\alpha$  fluxes are listed in Table 7, where line fluxes derived from spectral fits are given for the galaxies listed in Table 6 (i.e., those for which there were sufficient counts for spectral fitting in the Fe-K region). Note that the lines are typically about two orders-of-magnitude smaller than the flux of the strong K $\alpha$  line in NGC 6240.

Because the hard X-ray continua are so weak, the upper limits on the equivalent widths (EW) of the K $\alpha$  lines implied by the above are usually of-order a keV. The spectra of IRAS 05189-2524 and Mkn 231 have equivalent width upper limits of 0.1 keV and 0.5 respectively for a narrow K $\alpha$  line ( $\sigma = 0.01$  keV) at 6.4 keV. Note that in the cases of UGC 05101, IRAS 17208-0014 and IRAS 20551-4250, insufficient counts exist in the 3-8 keV bandpass to even fit the power-law plus Gaussian model.

In general, obscured (narrow-line) AGN in which the hard X-ray emission is dominated by reflection/reprocessing tend to have lines with EWs in excess of 1 keV (e.g., Ptak et al. (1996) and references therein), and similarly hot gas is expected to have Fe-K $\alpha$  emission at 6.7 keV with an equivalent width of  $\sim 0.6(Z/Z_\odot)$  keV (Rothenflug & Arnaud 1985). Thus, in most cases

TABLE 3. EXTRA-NUCLEAR POINT SOURCES

| Galaxy          | Position              | Offset<br>("'/kpc) | Counts | $F_{2-10}$ keV<br>$10^{-15}$ erg cm $^{-2}$ s $^{-1}$ | $L_{2-10}$ keV<br>$10^{40}$ erg s $^{-1}$ | Notes            |
|-----------------|-----------------------|--------------------|--------|---|---|------------------|
| Arp 220         | 15 34 57.0 23 30 5.6  | 7.3/2.8            | 29.2   | 1.8   | 0.13                                      |                  |
| IRAS 20551-4250 | 20 58 26.5 -42 39 8.6 | 8.4/7.5            | 87.6   | 6.9   | 2.8                                       |                  |
| IRAS 23128-5919 | 23 15 46.7 -59 3 11.0 | 4.7/4.0            | 75.5   | 6.4   | 2.9                                       | Northern nucleus |
| UGC 05101       | 9 35 52.7 61 21 12.3  | 8.3/6.8            | 17.5   | 1.2   | 0.42                                      |                  |

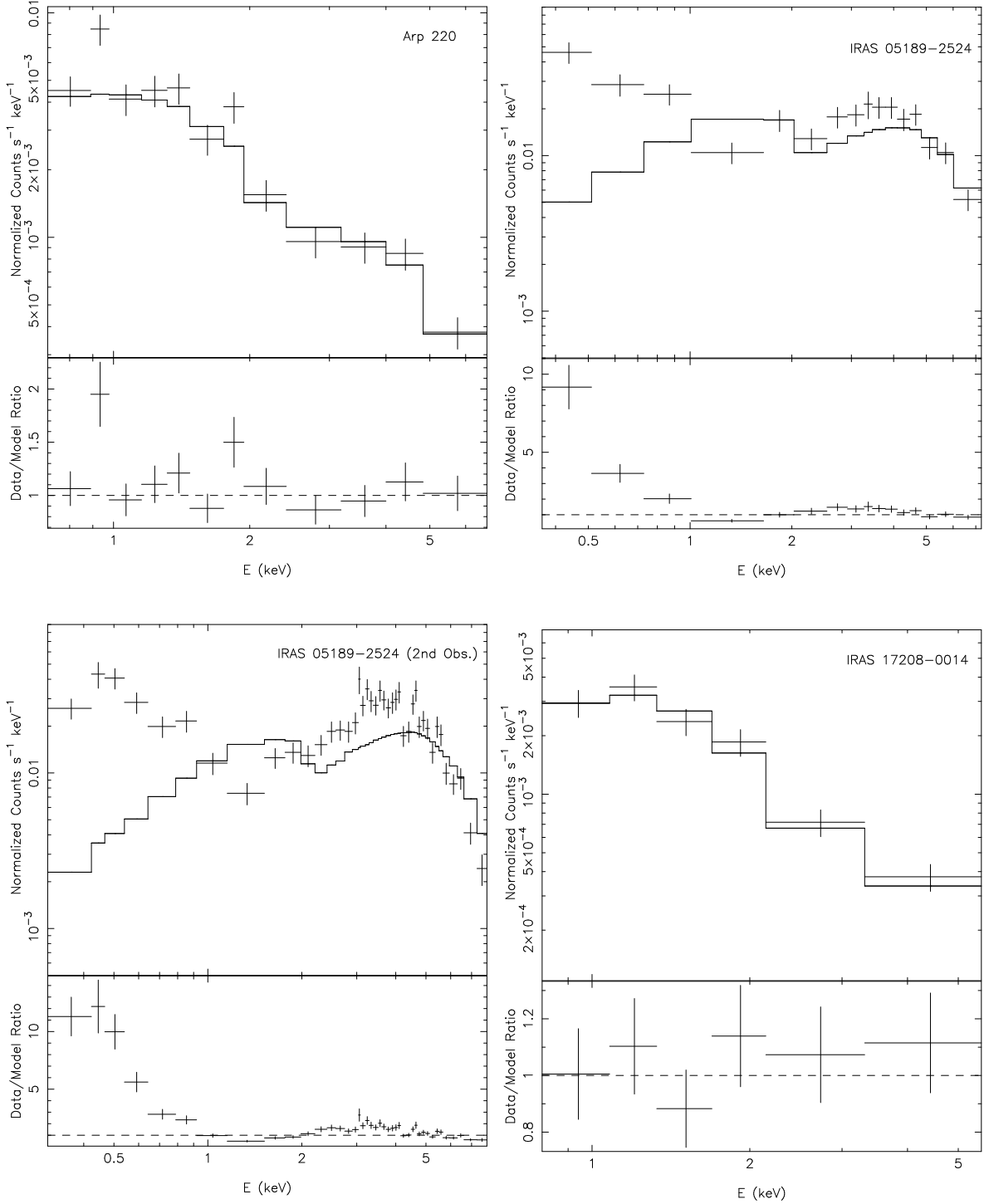


FIG. 2.—

the upper bounds on the EW are not terribly restrictive.

The upper limits on the  $K\alpha$  fluxes are more constraining



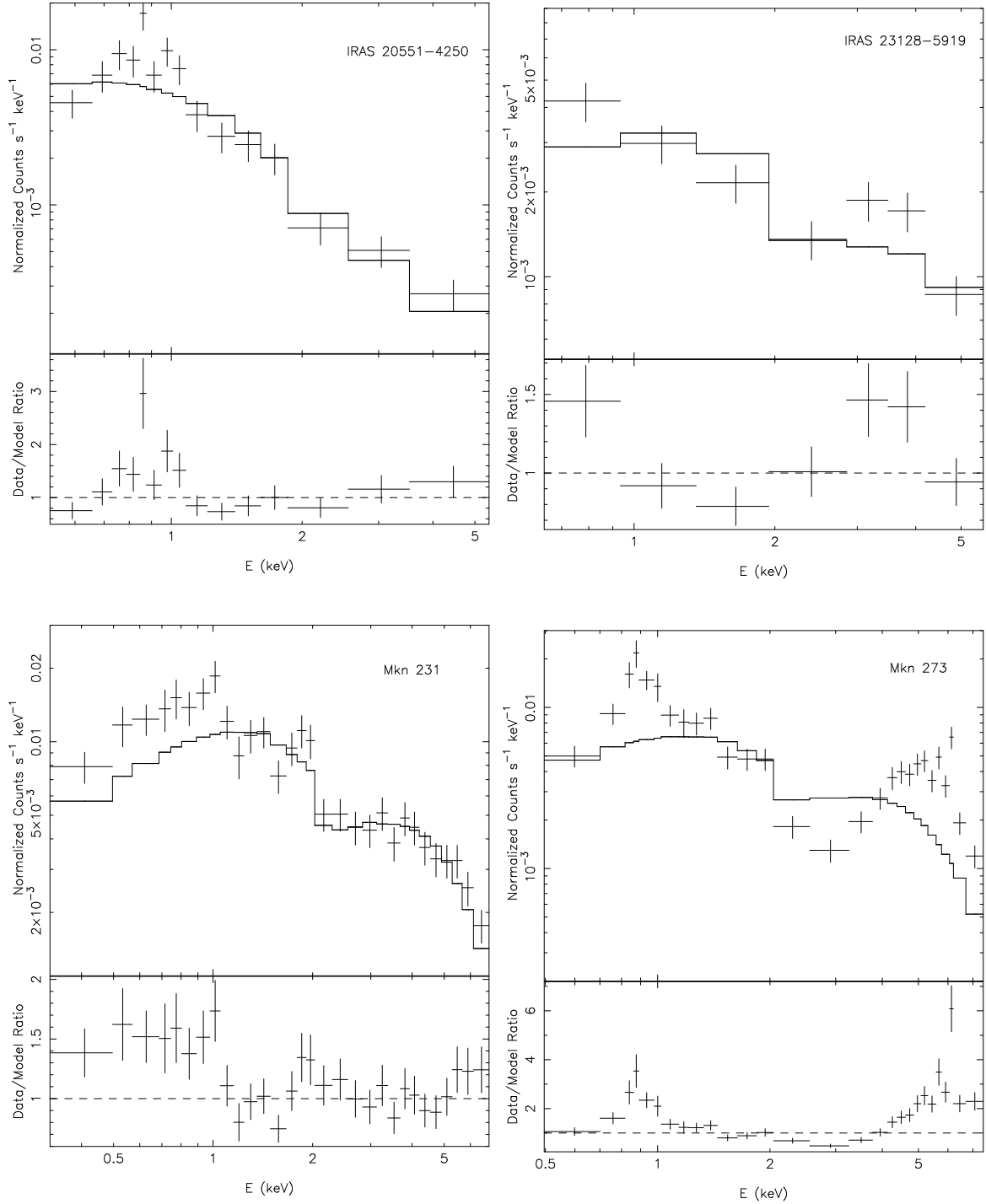


FIG. 2.— (cont.)

in these cases (as we will discuss below).

#### 4.2. More Complex Models

The reduced  $\chi^2$  values of plasma + power-law + Fe-K line fits to Mkn 273, NGC 6240, and UGC 05101 are  $\gtrsim 1.5$ . In the case of UGC 05101 the fit is nevertheless statistically acceptable due to the low number of degrees of freedom. We added an additional plasma model (mekal) model to the Mkn 273 and NGC 6240 fits. In the case of Mkn 273 this results in an accept-

able fit with  $\chi^2/dof = 41.2/40$ , however the photon index of the power-law component is poorly constrained  $\Gamma = 1.7$  (0.3 – 3.8). Since a motivation for these spectral fits is to compute accurate fluxes for comparison with global (i.e., spatially-averaged) spectral fits (see below), we fixed the photon index at 1.8, and the results of this fit are shown in Table 8. For NGC 6240 a more complex model was necessary in order to fit both the nuclear and global spectrum. This model, motivated by the BeppoSAX fit given in Vignati et al. (1999), contains

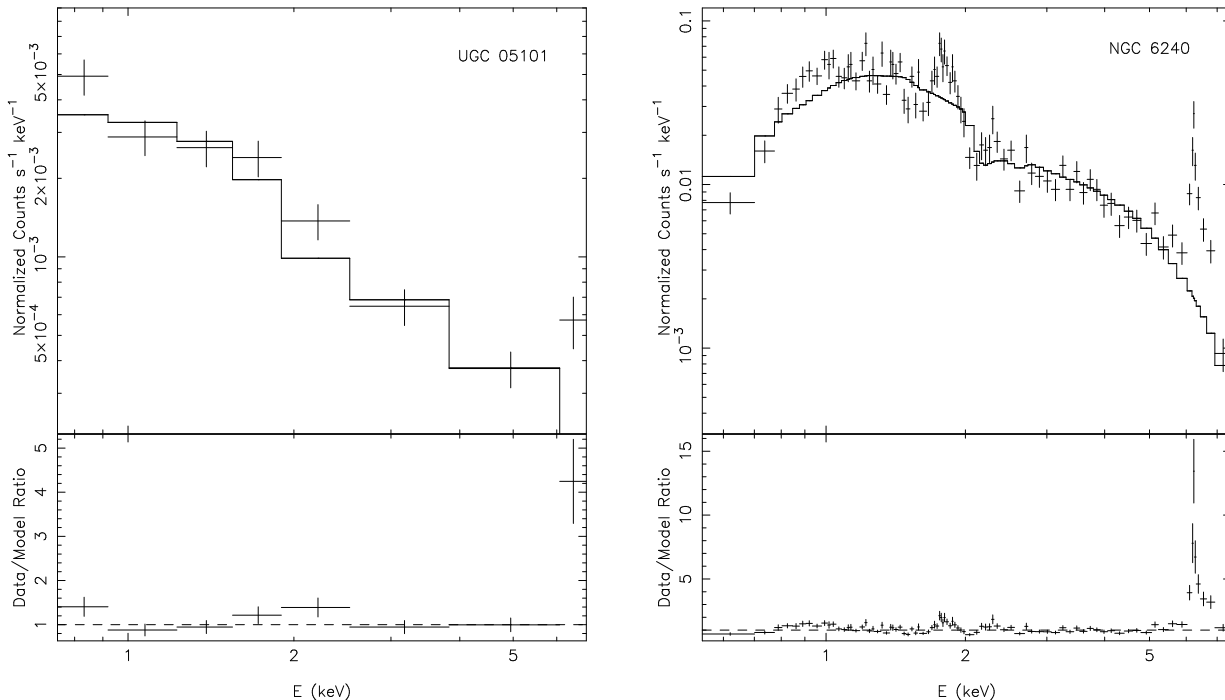


FIG. 2.— Power-law fits to the nuclear spectra of the ULIRG galaxies. The top panel shows the data and model and the data/model ratio is shown in the bottom panel.

TABLE 4. POWER-LAW FITS TO NUCLEAR SPECTRA

| Galaxy           | $N_H$ ( $10^{22}$ cm $^{-2}$ ) | $\Gamma$         | $\chi^2/\text{dof}$ |
|------------------|--------------------------------|------------------|---------------------|
| Arp 220          | 0.0                            | 0.9              | 39.5/21             |
| IRAS 05189-2524  | 0.0                            | -0.4             | 127/28              |
| IRAS 05189-2524* | 0.0                            | -0.7             | 430.2/78            |
| IRAS 17208-0014  | 0.3 (< 0.6)                    | 1.7 (1.0-2.3)    | 10.5/9              |
| IRAS 20551-4250  | 0.1                            | 2.0              | 30.9/12             |
| IRAS 23128-5919  | 0.0                            | 0.4              | 20.4/11             |
| Mkn 231          | 0.01 (<0.02)                   | 0.44 (0.33-0.53) | 57.0/53             |
| Mkn 273          | 0.0                            | 0.3              | 302/49              |
| UGC 05101        | 0.0                            | 1.0              | 35.5/12             |
| NGC 6240         | 0.39                           | 1.4              | 431/136             |

\*2nd observation

two plasma components, a power-law (representing AGN emission scattered by a scattering region), an Fe-K complex (modeled with multiple Gaussian components) and a Compton reflection component (Magdziarz & Zdziarski 1995). See Table 9 for the fit parameters. We also found it necessary to include an additional Gaussian component with an observed (rest-frame) energy of  $\sim 2.2$  ( $\sim 2.3$ ) keV, however note that the observed energy is close to the energies of significant absorption edges in the Chandra mirror response where the calibration tends to be the most uncertain, and accordingly this feature may not be real.

#### 4.3. Spatially-Averaged Spectra

In order to determine the amount of flux extended beyond the nuclear region we fitted the spectra extracted from the “global” regions shown in Figure 1 with a models consisting of a plasma plus absorbed power-law (i.e.,

as fit to the nuclear spectra) and two plasmas and an absorbed power-law. The parameters from the statistically-preferred model (based on the f-test statistic) are given in Table 10. The spectra from Mkn 273 and NGC 6240 were fit with the same models used for the nuclear spectra, with the results shown in Tables 8 and 9.

#### 4.4. Continuum Fluxes and Luminosities

The observed fluxes and luminosities in the 0.5-2.0 keV and 2.0-10.0 keV bandpasses are given in Table 11, derived from the plasma + power-law fits to the nuclear spectra, except for Mkn 273, UGC 05101 and NGC 6240 where the fit in Table 6 was used. We also include the fluxes derived from fits to the “global” spectra (using the models shown in Tables 8 - 10), from which it can be seen that on average  $\sim 50\%$  and  $75\%$  of the 0.5-2.0 keV and 2.0-10.0 keV total flux originates in the  $\sim 0.5 - 1.0$  kpc scale nuclear regions. Since the sources with higher signal-to-noise require more complex models to fit their spectra it is likely that most or all ULIRGs are similarly complex (see, e.g., XMM-Newton spectral fits in Braito et al. 2002). Fitting the spectra with models that are not sufficiently complex physically but are acceptable statistically may result in incorrect flux estimates, especially in the case of the 2-10 keV flux estimates when the power-law slope is poorly constrained. In order to derive a model-independent estimate of the amount of extra-nuclear flux we also list in Table 11 the ratio of the nuclear and global count rates in the 0.5-2.0 and 2.0-8.0 keV bandpasses (with the 2.0-8.0 keV count rate ratios being listed with the 2-10 keV flux ratios). As expected the flux and count rates ratio are in fairly good agreement, but differ by up to  $\sim 20\%$ .

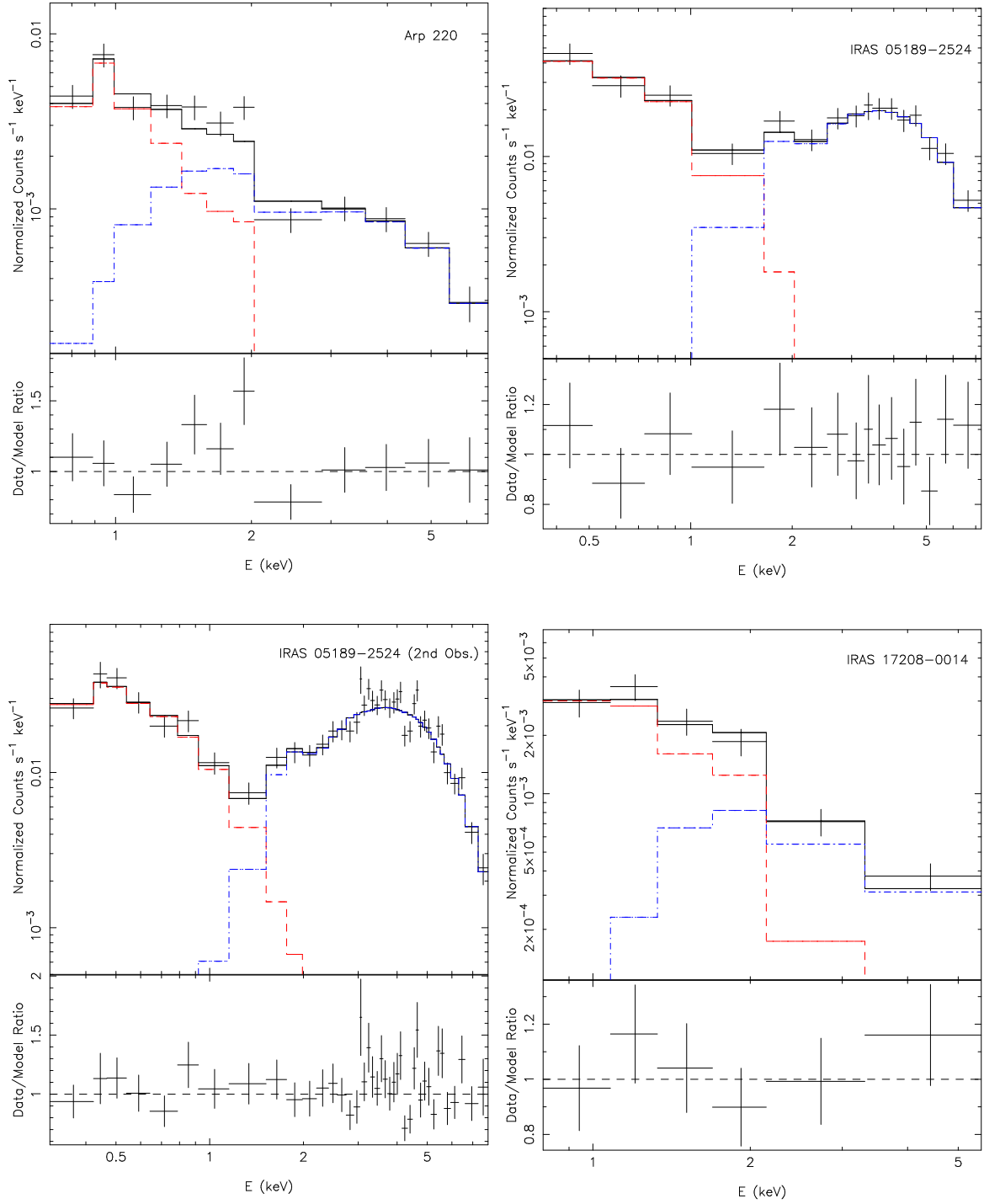


FIG. 3.—

Significant short-term variability in the 2.0-8.0 keV bandpass is not observed in the events extracted from the nuclear regions when tested by comparing the source and background photon arrival times with the K-S statistic, with the exception of Mkn 231 (Gallagher et al. 2002). In Figure 4 we plot the long-term 2-10 keV light curves of the ULIRGs for which ASCA and/or BeppoSAX data exist (listed in Table 12). The Chandra fluxes were derived from fits to the “global” regions shown in Figure 1, while the typical ASCA and BeppoSAX source

regions were 4-6'. For the ASCA observation of UGC 05101 and the two BeppoSAX observations of Arp 220, the source was not detected with sufficient counts for spectral modeling so the count rate was determined from the images and 2-10 keV fluxes were derived assuming the best-fitting spectral model to the Chandra data. While there is some apparent variability in IRAS 17208-0014 and IRAS 20551-4250, we note that the total flux of all sources detected within the central 4' of the Chandra observations of these galaxies was  $1.6 \times 10^{-13} \text{ erg cm}^{-2}$

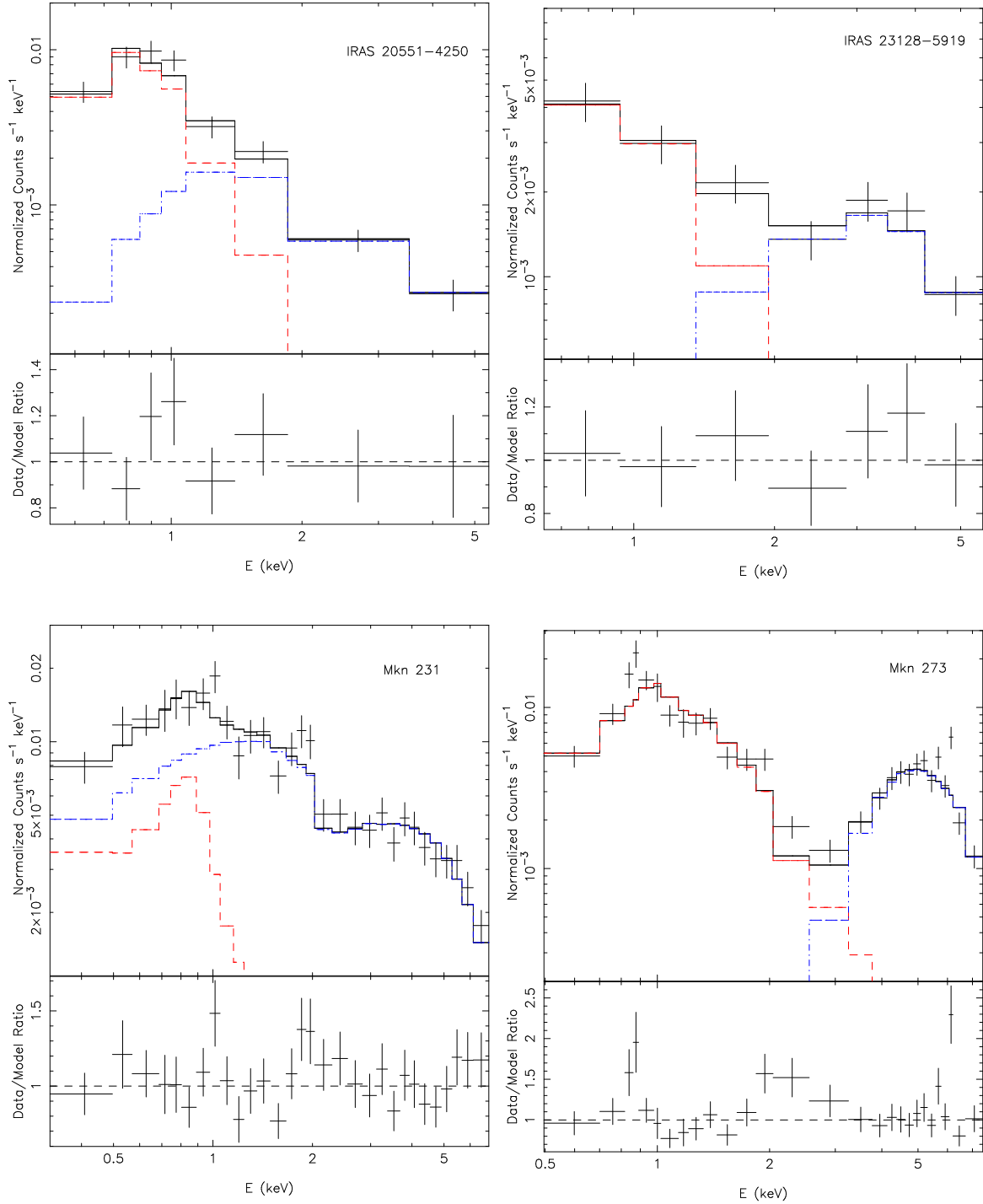


FIG. 3.— (cont.)

$s^{-1}$  and  $4.6 \times 10^{-13} \text{ erg cm}^{-2} s^{-1}$ , respectively. This suggests that some or all of the observed variability is due to source confusion in the ASCA data. In summary, hard X-ray variability is clearly observed in IRAS 05189-2524, Mkn 231, and Mkn 273 (the AGN ULIRGs) and in NGC 6240 at levels of  $\sim 40\%$  or greater, while in the remaining ULIRGs no variability is observed that is not possibly due to aperture effects.

## 6. DISCUSSION

Our overall goal in this paper is to better understand the role of AGN in the ULIRG phenomenon. We can cast this in terms of three related questions: 1) Is the signature of an AGN present in the Chandra hard X-ray data? 2) Does an AGN dominate the hard X-ray emission? 3) Do the X-ray data imply that an obscured AGN dominates the bolometric energy output? To address these questions, we will consider the structure/morphology of the X-ray emission (information that Chandra uniquely provides), the spectral properties of the emission, and the

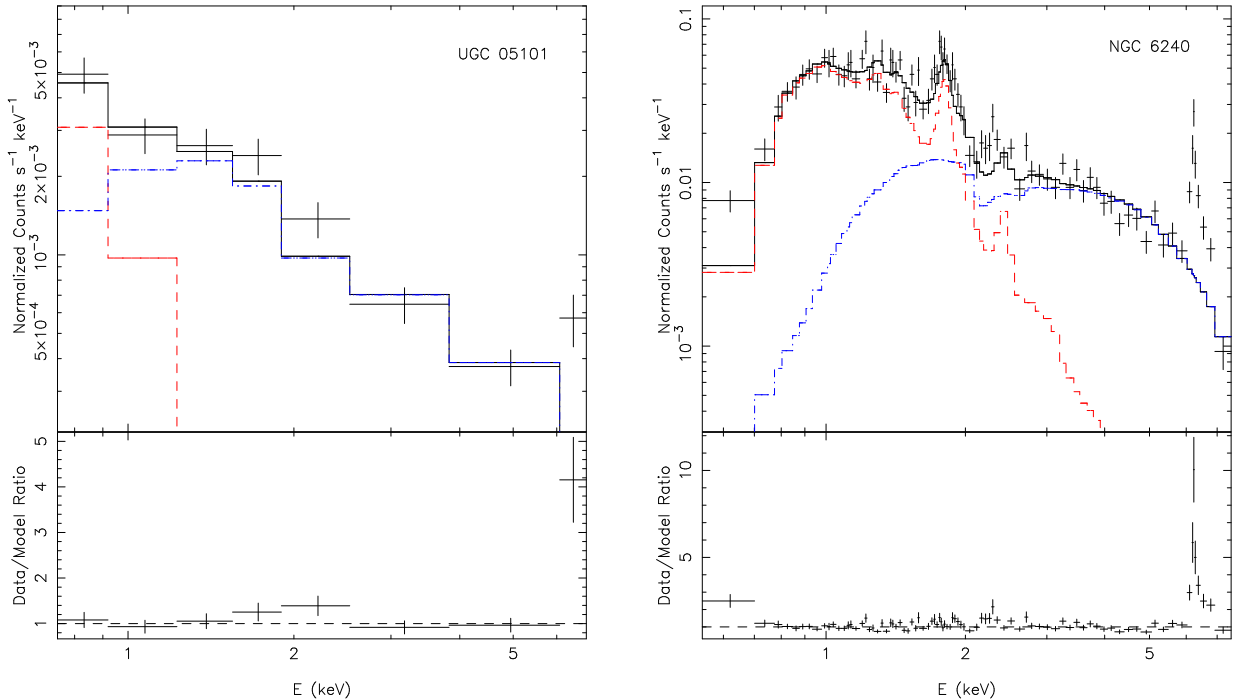


FIG. 3.— Plasma + power-law fits to the nuclear spectra of the ULIRG galaxies. The top panel shows the data and model and the data/model ratio is shown in the bottom panel. The plasma component model is shown with a dashed red line and the power-law component model is shown with a dot-dashed blue line.

TABLE 5. PLASMA + POWER-LAW FITS TO NUCLEAR SPECTRA

| Galaxy           | $N_H$<br>( $10^{22}$ cm $^{-2}$ ) | kT (keV)<br>(keV) | $Z/Z_\odot$       | $K^{**}$       | $N_{H,2}$<br>( $10^{22}$ cm $^{-2}$ ) | $\Gamma$      | $\chi^2/dof$ |
|------------------|-----------------------------------|-------------------|-------------------|----------------|---------------------------------------|---------------|--------------|
| Arp 220          | 0.6 (< 1.1)                       | 0.8 (0.6-1.1)     | 2.1 (>0.2)        | 1.3 (0.1 - 16) | 0.3 (<2.5)                            | 1.1 (0.3-1.8) | 19.5/17      |
| IRAS 05189-2524  | 0.01 (< 0.3)                      | 0.7 (<1.3)        | 0.01 (< 0.05)     | 24. (15.-250)  | 3.8 (2.2-6.0)                         | 1.0 (0.4-1.7) | 22.0/24      |
| IRAS 05189-2524* | 0.06 (< 0.2)                      | 0.4 (<0.8)        | 0.00 (< 0.03)     | 43. (16.-140)  | 4.5 (3.4-5.8)                         | 1.1 (0.7-1.5) | 87/74        |
| IRAS 17208-0014  | 1.0 (< 1.5)                       | 0.7(f)            | 1.0(f)            | 4.5 (<13.)     | 0.6 (<39)                             | 1.9 (> 0.5)   | 6.8/7        |
| IRAS 20551-4250  | 0.6 (<0.8)                        | 0.3 (< 1.0)       | 1.0(f)            | 8.2 (0.6-21.)  | 0.0 (<4.0)                            | 1.6 (0.8-3.8) | 11.2/9       |
| IRAS 23128-5919  | 0.2 (< 0.5)                       | 0.7(f)            | 0.0 (< 0.1)       | 9.0 (2.5-18)   | 4.8 (0.9-13.2)                        | 2.2 (0.5-4.6) | 8.0/8        |
| Mkn 231          | 0.0 < 0.6)                        | 0.7(f)            | 0.15 (0.02 - 3.2) | 1.8 (0.2-16)   | 0.0 (< 0.6)                           | 0.2 (0.0-0.5) | 41.6/50      |
| Mkn 273          | 0.3                               | 1.3               | 0.06              | 17             | 24                                    | 0.8           | 72.6/45      |
| UGC 05101        | 0.2                               | 0.4               | 1.0(f)            | 5.6            | 0.3                                   | 1.2           | 29.3/9       |
| NGC 6240         | 1.15                              | 0.65              | 0.58              | 300.           | 0.                                    | 0.80          | 321/132      |

NOTE. — Errors were determined using  $\Delta\chi^2 = 4.605$  for fits with  $\chi^2/dof < 1.5$ . Parameters marked with “f” were frozen at the value shown.

\*2nd observation

\*\*Plasma model normalization in units of  $10^{-9} \frac{n_e n_H dV}{4\pi D^2}$ ,  $n_e$  = electron density in cm $^{-3}$ ,  $n_p$  = Hydrogen density in cm $^{-3}$ ,  $D$  = luminosity distance to source in cm.

ratio of the hard X-ray to bolometric (IR) luminosity.

As noted in section 1, optical and IR spectroscopy of ULIRGs reach a surprising degree of agreement as to their classification. ULIRGs that are optically classified as HII-regions or LINERs (type 1 or type 2 Seyferts) are nearly always classified as starbursts (AGN) on the basis of mid-IR spectroscopy (Lutz, Veilleux, & Genzel 1999; Taniguchi, Yoshino, Ohya, & Nishiura 1999). Near-IR spectroscopy is also available for much of the sample, and provides further diagnostic information, such as identifying AGN on the basis of detection of broad Pa $\alpha$  or [Si VI] (Veilleux, Sanders, & Kim 1999) and the strength of PAH emission and absorption features (Imanishi & Dudley 2000). Finally, AGN can be dis-

criminated from starbursts (on an empirical, statistical basis) using the  $F_{25\mu m}/F_{60\mu m}$  flux ratio, which is a measure of dust temperature (de Grijp, Miley, & Lub 1987). This information is summarized in Table 13. On the basis of these diagnostics, 5 ULIRGs are classified as starbursts (Arp 220, UGC 5101, IRAS 17208-0014, IRAS 20551-4250, and IRAS 23128-5919), and the other three are classified as AGN (Mkn 231, Mkn 273, and IRAS 05189-2524). The analysis of a 3-4 $\mu m$  spectrum presented by Imanishi, Dudley & Maloney (2001) shows that a highly-obscured AGN is likely to be present in UGC 05101. In what follows below, we will refer to these two classes as “starburst-ULIRGs” and “AGN-ULIRGs” respectively (for consistency we place UGC

TABLE 6. FE-K FITS TO NUCLEAR SPECTRA

| Galaxy      | Bandpass (keV) | $N_H$ ( $10^{22}$ cm $^{-2}$ ) | $\Gamma$       | Line E (keV)     | Line $\sigma$ (keV) | Line EW (keV)    | $\chi^2/\text{dof}$ |
|-------------|----------------|--------------------------------|----------------|------------------|---------------------|------------------|---------------------|
| IRAS 05189* | 0.4-8.0        | 4.5 (3.4-5.8)                  | 1.1 (0.7-1.5)  | 6.4f             | 0.01f               | 0.0 (<0.1)       | 87/73               |
|             | 2.0-8.0        | 4.4 (2.4-6.7)                  | 1.1 (0.6-1.7)  | 6.4f             | 0.01f               | 0.0 (<0.1)       | 73/57               |
|             | 2.0-8.0        | 4.8 (2.7-7.2)                  | 1.3 (0.7-1.9)  | 6.7f             | 0.1f                | 0.1 (<0.4)       | 71/57               |
|             | 2.0-8.0        | 4.7 (2.5-7.6)                  | 1.2 (0.6-2.1)  | 6.7f             | 0.5f                | 0.1 (<0.7)       | 73/57               |
| Mkn 231     | 0.4-8.0        | 0 (<0.8)                       | 0.2 (0.0-0.7)  | 6.4f             | 0.01f               | 0.2 (<0.5)       | 38/49               |
|             | 2.0-8.0        | 0.0 (<1.6)                     | 0.3 (0.0-0.9)  | 6.4f             | 0.01f               | 0.2 (<0.6)       | 12/24               |
|             | 2.0-8.0        | 0.0 (<1.5)                     | 0.3 (-0.1-0.9) | 6.7f             | 0.1f                | 0.1 (<0.5)       | 16/24               |
|             | 2.0-8.0        | 0.0 (<2.3)                     | 0.5 (0.0-1.3)  | 6.7f             | 0.5f                | 0.6 (<1.5)       | 13/24               |
| Mkn 273     | 0.4-8.0        | 24 (9-40)                      | 0.9 (-0.5-2.6) | 6.35 (6.30-6.39) | 0.01 (<0.08)        | 0.24 (0.09-0.44) | 61/42               |
| UGC 05101   | 0.4-8.0        | 1.0 (<6.5)                     | 1.9 (0.80-4.7) | 6.32 (6.27-6.44) | 0.01f               | 5.9 (2.7-630)    | 15/8                |
| NGC 6240    | 0.4-8.0        | 0.4 (<1.9)                     | 1.4 (0.9-1.9)  | 6.46 (6.39-6.57) | 0.20 (0.10-0.36)    | 2.4 (1.7-3.2)    | 217/129             |

NOTE. — Fits to the 2.0-8.0 keV bandpass are based on the model given in Table 5 with the addition of a Gaussian component with the parameters shown here for the second (i.e., intrinsic) absorber, power-law slope and Gaussian line. Fits to the 3.0-8.0 keV bandpass are based on an absorbed power-law plus Gaussian line model.

\*Second observation

TABLE 7. CHANDRA FE-K LINE LIMITS

| Galaxy     | $F_{\text{Fe-K}}$ ( $10^{-14}$ ergs s $^{-1}$ ) | Method             |
|------------|---|--------------------|
| Arp 220    | <0.92   | Direct measurement |
| IRAS 05189 | <5.3  | Spectral fit       |
| IRAS 17208 | <0.83   | Direct measurement |
| IRAS 20551 | <0.88   | Direct measurement |
| IRAS 23128 | <1.3  | Direct measurement |
| Mkn 231    | <5.0  | Spectral fit       |
| Mkn 273    | 6.0 (2.2-11)                                    | Spectral fit       |
| UGC 05101  | 3.5 (1.6-380)                                   | Spectral fit       |
| NGC 6240   | 30. (22.-40.)                                   | Spectral fit       |

\*Method used to determine the Fe-K flux, as described in the text. Briefly, for sources with insufficient counts for spectral fitting, “direct measurement” refers to determining an upper-limit to the Fe-K flux based on the background level at 6.4 keV in the rest frame.

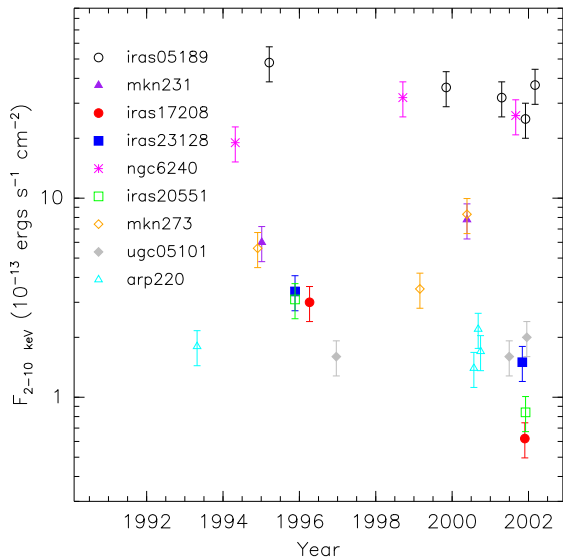


FIG. 4.— Long-term light curves of ULIRG sample.

05101 in the starburst-ULIRG category), bearing in mind that *this empirical classification may not reflect*

TABLE 8. DOUBLE PLASMA + POWER-LAW FITS TO MKN 273 SPECTRA

| Parameter                          | Nuclear Spectrum          | Global Spectrum           |
|------------------------------------|---------------------------|---------------------------|
| $N_{H,1}$ ( $10^{20}$ cm $^{-2}$ ) | 0.5 (< 1.8)               | 2.1 (<7.8)                |
| $kT_1$ (keV)                       | 0.84 (0.68-0.97)          | 0.66 (0.59-0.71)          |
| $Z_1$ ( $/Z_\odot$ )               | 1.0f                      | 0.15 (0.10-0.23)          |
| $K_1^*$                            | 0.75 (0.50-1.4)           | 17 (1.1-31)               |
| $N_{H,2}$ ( $10^{22}$ cm $^{-2}$ ) | 1.2 (0.7-1.9)             | 1.3 (0.9-2.2)             |
| $kT_2$ (keV)                       | 1.7 (1.0-2.0) $^\ddagger$ | 1.1 (0.87-1.4)            |
| $Z_2$ ( $/Z_\odot$ )               | 1.0f                      | 0.9 (0.1-5.0) $^\ddagger$ |
| $K_2^*$                            | 12 (8.4-20)               | 22 (4.5-64)               |
| $N_{H,3}$ ( $10^{23}$ cm $^{-2}$ ) | 3.5 (3.0-4.3)             | 3.4 (2.7-4.2)             |
| Line E (keV)                       | 6.35 (6.30-6.39)          | 6.37 (6.30-6.42)          |
| Line $\sigma$ (keV)                | 0 (< 0.08)                | 0.0 (< 0.10)              |
| Line $N^\dagger$                   | 7.2 (2.6-11.8)            | 7.2 (2.2-13)              |
| $\Gamma$                           | 1.8f                      | 1.8f                      |
| $N$ ( $\times 10^4$ )              | 7.4 (5.9-9.6)             | 7.6 (5.7-10)              |
| $\chi^2/\text{dof}$                | 41.2/41                   | 118/103                   |

NOTE. — The model fitted to the spectra was:  $Abs(N_{H,1})[Mekal(kT_1, Z_1, K_1) + Abs(N_{H,2}) \times Mekal(kT_2, Z_2, K_2) + Abs(N_{H,3}) \times (PL(\Gamma, N) + Gaussian(E, \sigma, N_{Line}))]$ , with Abs = absorption, Mekal=plasma, PL = power law and Gaussian = Gaussian components.

\*Plasma normalization in units of  $10^{-9} \frac{\int n_e n_H dV}{4\pi D^2}$ ,  $n_e$  = electron density in cm $^{-3}$ ,  $n_p$  = Hydrogen density in cm $^{-3}$ , D = luminosity distance to source in cm.

$^\dagger$ Gaussian line normalization in units of  $10^{-6}$  photons cm $^{-2}$  s $^{-1}$ .

$^\ddagger$ Parameter reached pre-set boundary during error search.

*the true nature of the dominant energy source.* For example, it is fairly clear that an AGN contributes substantially to the hard X-ray emission from NGC 6240 (Iwasawa & Comastri 1998; Vignati et al. 1999) even though it is an optical LINER that appears starburst-dominated in the infrared (Imanishi & Dudley 2000; Lutz, Veilleux, & Genzel 1999). We will see below that the AGN- and starburst-ULIRGs do differ significantly in their hard X-ray properties.

### 6.1. Morphology

In every case, significant hard X-ray emission is present in the nuclear region. In general, the hard X-ray nuclei are within 0.5-1.5'' of radio and CO nuclear posi-

TABLE 9. COMPLEX SPECTRAL FITS TO NGC 6240 SPECTRA

| Parameter                          | Nuclear Spectrum           | Global Spectrum  |
|------------------------------------|----------------------------|------------------|
| $N_{H,1}$ ( $10^{21}$ cm $^{-2}$ ) | 0.4 (<5.5)                 | 0.5 (0.3-0.9)    |
| $N_{H,2}$ ( $10^{21}$ cm $^{-2}$ ) | 5.4 (<9.4)                 | 0.3 (<1.5)       |
| $kT_1$ (keV)                       | 0.23 (0.17-0.38)           | 0.30 (0.27-0.33) |
| $Z_1$ ( $/Z_{\odot}$ )             | 2.6 (0.1-5.0) <sup>‡</sup> | 0.32 (0.11-1.1)  |
| $K_1^*$                            | 0.51 (0.04-1.9)            | 4.1 (1.3-13.)    |
| $N_{H,3}$ ( $10^{22}$ cm $^{-2}$ ) | 1.3 (0.77-1.4)             | 0.78 (0.69-0.90) |
| $kT_2$ (keV)                       | 0.67 (0.61-0.76)           | 0.66 (0.62-0.72) |
| $Z_2$ ( $/Z_{\odot}$ )             | 9.0 (3.1-10) <sup>‡</sup>  | 0.76 (0.32-1.23) |
| $K_2^*$                            | 1.3 (0.88-3.9)             | 21 (3.5-41.)     |
| Line1 E (keV)                      | 2.31 (2.25-2.35)           | 2.33 (2.31-2.35) |
| Line1 $\sigma$ (keV)               | 0.01f                      | 0.01f            |
| Line1 N $^{\dagger}$               | 5.4 (2.0-9.0)              | 12. (7.2-16)     |
| $N_{H,4}$ ( $10^{22}$ cm $^{-2}$ ) | 1.5 (0.5-2.3)              | 1.1 (0.7-1.7)    |
| $\Gamma$                           | 1.55 (0.98-2.02)           | 1.62 (1.22-1.93) |
| $N$ ( $\times 10^4$ )              | 1.8 (0.9-3.5)              | 2.7 (1.3-4.2)    |
| Line2 E (keV)                      | 6.35 (6.33-6.38)           | 6.34 (6.31-6.37) |
| Line2 $\sigma$ (keV)               | 0.00 (<0.06)               | 0.02 (<0.08)     |
| Line2 N $^{\dagger}$               | 16 (11-21)                 | 17 (11-24)       |
| Line3 E (keV)                      | 6.57 (6.50-6.69)           | 6.62 (6.54-6.67) |
| Line3 $\sigma$ (keV)               | 0.01 (< 0.20)              | 0.01 (<0.13)     |
| Line3 N $^{\dagger}$               | 4.9 (0.8-11)               | 7.4 (2.2-13)     |
| $N_{H,5}$ ( $10^{24}$ cm $^{-2}$ ) | 1.3 (0.5-3.0)              | 1.3 (0.7-2.3)    |
| $N_{refl}$                         | 2.5 (0.5-5.7)              | 4.6 (1.4-13)     |
| $\chi^2/dof$                       | 147/117                    | 331/225          |

NOTE. — The model fitted to the spectra was:  $Abs(N_{H,1}) \times [Abs(N_{H,2}) \times Mekal(kT_1, Z_1, K_1) + Abs(N_{H,2}) \times [Mekal(kT_2, Z_2, K_2) + Gaussian(E_1, \sigma_1, N_{Line,1}) + Abs(N_{H,3}) \times [PL(\Gamma, N) + Gaussian(E_2, \sigma_2, N_{Line,2}) + Gaussian(E_3, \sigma_3, N_{Line,3})] + Abs(N_{H,4}) \times Refl(N_{refl})]$ , with Abs = absorption, Mekal=plasma, PL = power law, Gaussian = Gaussian components and Refl = Compton reflection components.

\*Plasma normalization in units of  $10^{-10} \frac{f n_e n_H dV}{4\pi D^2}$ ,  $n_e$  = electron density in cm $^{-3}$ ,  $n_H$  = Hydrogen density in cm $^{-3}$ , D = luminosity distance to source in cm.

$^{\dagger}$ Gaussian line normalization in units of  $10^{-6}$  photons cm $^{-2}$  s $^{-1}$ .

$^{\ddagger}$ Parameter reached pre-set boundary during error search.

tions (Bryant & Scoville 1999; Condon et al. 1991, 1996; Planesas, Mirabel, & Sanders 1991; Scoville et al. 1991; Thean et al. 2000; Yun & Scoville 1995). However, as noted above, in three cases (the starburst-ULIRGs Arp 220, and IRAS 17208-0014) and in NGC 6240, this component is resolved on arcsecond ( $\sim$  kpc) scales (see also Komossa et al. 2003). In the other six cases where the nuclear source is unresolved, the upper limit to the size ( $\sim$  0.5 kpc FWHM) is consistent with either an AGN or compact starburst with a size similar to the nuclear radio continuum and CO emission (see Table 13 and references therein).

In addition to the nuclear emission, a somewhat surprising result is that often extended hard X-ray emission is detected beyond the nuclear region, on scales of order ten kpc. In five cases (the starburst ULIRGs IRAS 17208-0014, IRAS 20551-4250, IRAS 23128-5919, UGC 5101) and in NGC 6240, this large-scale emission comprises a significant fraction ( $\sim$  10 to 50%) of the total. Thus, in the five starburst-ULIRGs, the nuclear source is spatially resolved (two cases) and/or a significant fraction of the total hard X-ray emission arises well outside the nucleus (four cases). The nuclear source is unresolved and dominates the total hard X-ray emission in the three AGN-ULIRGs.

By way of comparison, Chandra observations of nearby

starburst galaxies such as M82 and NGC 253 have shown that a large fraction of the hard X-ray emission in these galaxies is due to point-sources, most likely high-mass X-ray binaries, concentrated within the central  $\sim$  kpc of the galaxy. Several of the ULIRGs have extra-nuclear sources that would qualify as ULXs if they are not interlopers. ULXs are often observed in starburst galaxies and, more notably for comparison with ULIRGS, in mergers such as the Antennae (Zezas & Fabbiano 2002). In IRAS 20551-4250  $\sim$  50% of the extra-nuclear hard X-ray flux may be due to a single ULX. The remainder of the hard X-ray emission in starbursts is due to an unresolved population of lower-luminosity X-ray binaries (Grimm, Gilfanov, & Sunyaev 2003), very hot gas ( $\geq$  few keV, see Cappi et al. 1999; Griffiths et al. 2000), or inverse-Compton scattering of IR photons off of relativistic electrons generated by supernova shocks (Moran, Lehnert, & Helfand 1999; Persic & Rephaeli 2002). A strong point source at the dynamical center of the galaxy (i.e. a plausible AGN candidate) is typically not detected (although cf., Weaver et al. 2002).

The hard X-ray morphology in these ULIRGs is generally consistent with these types of starbursts placed at the same distance as the ULIRG galaxies (even for the AGN-ULIRGs). Table 13 also lists the semimajor axis size of nuclear CO observed in several ULIRGs along with the hard X-ray semimajor axis derived from Gaussian x PSF fits to the hard X-ray surface brightness. These values are clearly consistent with the X-ray emission originating from within the nuclear molecular cloud/disk, or from a region of similar size (in the cases of Arp 220 and IRAS 17208-0014).

## 6.2. Spectroscopy

As stated above, most of the galaxies in this sample require at least two model components to fit their X-ray spectra. The soft X-ray spectra of these galaxies show that hot gas with  $kT \sim$  0.7 keV is present within the nuclei of these galaxies (with the possible exception of IRAS 05189-2524 where the AGN may be completely swamping any thermal flux). In this regard, they are very similar to typical starburst galaxies observed with Chandra (Lira, Ward, Zezas & Murray 2002; Martin, Kobulnicky, & Heckman 2002; Strickland et al. 2002).

The hard X-rays we observe may in principle be due to either an AGN or starburst. Our analysis shows that the hard X-ray emission detected in the ULIRGs is generally *not* absorbed by large column densities (i.e., in excess of  $10^{23}$  cm $^{-2}$ ). Mkn 273 is the only exception (see also Xia et al. 2002). If the hard X-rays are due to an AGN, then there are two possibilities: the AGN is truly unabsorbed (and hence has a low intrinsic luminosity) or the AGN is ‘‘Compton-thick’’ (i.e., absorbed by a column in excess of  $10^{24}$  cm $^{-2}$ ) and the observed hard X-rays are scattered into the line of sight. In the first case we would expect the hard X-ray slopes to be similar to those observed in Seyfert 1 and Compton-thin Seyfert 2 galaxies, namely  $\Gamma = 1.5-2.0$  (Dahlem, Weaver & Heckman 1998; Mushotzky, Done, & Pounds 1993; Ptak et al. 1999). IRAS 05189-2524 is consistent with this perspective, once we allow for the possible presence of Fe-K emission with an EW of  $\sim$  0.1 keV (see Table 6). On the other hand the

TABLE 10. FITS TO GLOBAL SPECTRA

| Parameter                           | Arp 220                   | I05189                    | I17208                  | I20551                    | I23128                  | Mkn 231                   | UGC 05101                |
|-------------------------------------|---------------------------|---------------------------|-------------------------|---------------------------|-------------------------|---------------------------|--------------------------|
| $N_{H,1}$ ( $10^{21}$ cm $^{-2}$ )  | 0.20 $^{+0.94}_{-0.00}$ ‡ | 1.39 $^{+0.48}_{-1.25}$   | 5.22 $^{+4.02}_{-4.72}$ | 0.20 $^{+2.82}_{-0.00}$ ‡ | 2.98 $^{+2.17}_{-1.11}$ | 0.05 $^{+0.79}_{-0.00}$ ‡ | 2.29 $^{+3.12}_{-2.14}$  |
| $kT_1$ (keV)                        | 0.33 $^{+0.06}_{-0.03}$   | 0.30 $^{+0.31}_{-0.00}$ ‡ | 0.35 $^{+0.96}_{-0.05}$ | 0.32 $^{+0.12}_{-0.02}$   | 0.50 $^{+0.19}_{-0.20}$ | 0.53 $^{+0.15}_{-0.23}$   | 0.70 $^{+0.34}_{-0.40}$  |
| $Z_1$ ( $/Z_\odot$ )                | 1.0f                      | 0.0 $^{+0.0}_{-0.0}$ ‡    | 0.1 $^{+4.9}_{-0.1}$    | 1.0f                      | 0.1 $^{+0.1}_{-0.0}$    | 0.2 $^{+0.3}_{-0.1}$      | 0.1 $^{+0.1}_{-0.0}$     |
| $K_1^*$                             | 1.20                      | 141.40                    |                         |                           |                         |                           |                          |
| $N_{H,2}$ ( $10^{22}$ cm $^{-2}$ )  | 0.7 $^{+0.2}_{-0.5}$      | 10.6 $^{+89.4}_{-8.8}$    |                         |                           |                         |                           |                          |
| $kT_2$ (keV)                        | 0.8 $^{+0.1}_{-0.2}$      | 2.0 $^{+0.0}_{-0.9}$ ‡    |                         |                           |                         |                           |                          |
| $Z_2$ ( $/Z_\odot$ )                | 1.0f                      | 0.6 $^{+4.4}_{-0.5}$      |                         |                           |                         |                           |                          |
| $K_2^*$                             | 8.84                      | 563.70                    |                         |                           |                         |                           |                          |
| $N_{H,3}$ ( $10^{22}$ cm $^{-2}$ )  | 1.0 $^{+2.9}_{-1.0}$      | 2.8 $^{+1.1}_{-0.5}$      | 0.0 $^{+6.2}_{-0.0}$ ‡  | 0.7 $^{+0.3}_{-0.6}$      | 5.1 $^{+6.8}_{-3.9}$    | 0.0 $^{+2.1}_{-0.0}$ ‡    | 0.7 $^{+4.6}_{-0.7}$     |
| $\Gamma$                            | 1.14 $^{+0.93}_{-0.87}$   | 0.52 $^{+0.55}_{-0.23}$   | 1.68 $^{+1.69}_{-1.22}$ | 0.85 $^{+2.04}_{-1.61}$   | 2.59 $^{+1.95}_{-1.31}$ | 0.55 $^{+0.37}_{-0.41}$   | 1.06 $^{+1.79}_{-1.01}$  |
| $N_3$ ( $\times 10^5$ )             | 1.38                      | 11.32                     | 1.53                    | 0.51                      | 21.59                   | 2.85                      | 0.80                     |
| Line E (keV)                        |                           |                           |                         |                           |                         |                           | 6.90 $^{+0.00}_{-0.29}$  |
| Line $\sigma$ (keV)                 |                           |                           |                         |                           |                         |                           | 0.37 $^{+0.13}_{-0.37}$  |
| Line N $^\dagger$ ( $\times 10^6$ ) |                           |                           |                         |                           |                         |                           | 4.53 $^{+68.60}_{-2.91}$ |
| $\chi^2/dof$                        | 48.9/64                   | 94.4/75                   | 18.7/16                 | 21.0/27                   | 30.7/30                 | 83.1/89                   | 32.5/16                  |

\* Plasma normalization in units of  $10^{-9} \frac{\int n_e n_H dV}{4\pi D^2}$ ,  $n_e$  = electron density in cm $^{-3}$ ,  $n_p$  = Hydrogen density in cm $^{-3}$ ,  $D$  = luminosity distance to source in cm.

† Gaussian line normalization in units of  $10^{-6}$  photons cm $^{-2}$  s $^{-1}$ .

‡ Parameter reached pre-set boundary during error search.

TABLE 11. FLUXES AND LUMINOSITIES

| Galaxy           | Global            |                |                | Nuclear           |                | 0.5-2.0 keV       |                   | 2-10 keV          |                   |
|------------------|-------------------|----------------|----------------|-------------------|----------------|-------------------|-------------------|-------------------|-------------------|
|                  | $F_{0.5-2.0}$ keV | $F_{2-10}$ keV | $L_{2-10}$ keV | $F_{0.5-2.0}$ keV | $F_{2-10}$ keV | $\frac{F_N}{F_G}$ | $\frac{C_N}{C_G}$ | $\frac{F_N}{F_G}$ | $\frac{C_N}{C_G}$ |
| Arp 220          | 0.6               | 1.3            | 0.10           | 0.16              | 1.2            | 0.27              | 0.25              | 0.85              | 0.65              |
| IRAS 05189-2524* | 0.73              | 37.            | 15.            | 0.66              | 35.            | 0.90              | 0.87              | 0.96              | 0.95              |
| IRAS 17208-0014  | 0.21              | 0.62           | 0.25           | 0.11              | 0.42           | 0.52              | 0.43              | 0.68              | 0.77              |
| IRAS 20551-4250  | 0.49              | 0.84           | 0.35           | 0.18              | 0.39           | 0.37              | 0.37              | 0.46              | 0.42              |
| IRAS 23128-5919  | 0.43              | 1.5            | 0.66           | 0.13              | 1.3            | 0.31              | 0.25              | 0.92              | 0.67              |
| Mkn 231          | 1.0               | 7.8            | 3.1            | 0.53              | 8.1            | 0.53              | 0.47              | 1.04              | 0.85              |
| Mkn 273          | 1.1               | 8.3            | 2.6            | 0.34              | 7.8            | 0.30              | 0.26              | 0.95              | 0.88              |
| UGC 05101        | 0.20              | 1.6            | 0.55           | 0.12              | 0.81           | 0.60              | 0.52              | 0.51              | 0.76              |
| NGC 6240         | 7.2               | 26.            | 3.4            | 1.8               | 17.            | 0.26              | 0.23              | 0.66              | 0.63              |

NOTE. — Fluxes are in units of  $10^{-13}$  erg cm $^{-2}$  s $^{-1}$ , luminosities are in units of  $10^{42}$  erg s $^{-1}$ , derived from plasma plus power-law fits. The “nuclear” 2-10 keV flux exceeds the “global” flux in Mkn 231 due to statistical uncertainty in the power-law slope; the global 2-10 keV flux of Mkn 231 is  $8.9 \times 10^{-13}$  erg cm $^{-2}$  s $^{-1}$  when the power-law slope is fixed at best-fit value of the nuclear spectrum fit ( $\Gamma = 0.21$ ).  $\frac{F_N}{F_G}$  is the ratio of nuclear and global fluxes while  $\frac{C_N}{C_G}$  is the ratio of nuclear and global count rates.

TABLE 12. ASCA AND BEPPoSAX FLUXES AND FE-K LINE LIMITS

| Galaxy          | Satellite | Date       | $F_{0.5-2.0}$ keV | $F_{2-10}$ keV | Fe-K Line EW (keV) | References |
|-----------------|-----------|------------|-------------------|----------------|--------------------|------------|
| Arp 220         | ASCA      | 03/27/1994 | 0.6               | 1.8            | ...                | 1          |
| Arp 220         | BeppoSAX  | 08/04/2000 | ...               | 2.2            | ...                | 7          |
| Arp 220         | BeppoSAX  | 08/27/2000 | ...               | 1.7            | ...                | 7          |
| Mkn 231         | ASCA      | 12/05/1994 | 1.2               | 6.0            | < 0.9              | 1          |
| Mkn 273         | ASCA      | 10/27/1994 | 1.6               | 5.6            | 0.52 (0.26-1.0)    | 1          |
| Mkn 273         | BeppoSAX  | 01/25/1999 | ...               | 3.5            | 1.2 (0.2-3.2)      | 2          |
| IRAS 05189-2524 | ASCA      | 02/15/1995 | ...               | 48             | 0.11 (0.03-0.18)   | 4          |
| IRAS 05189-2524 | BeppoSAX  | 10/03/1999 | ...               | 36             | 0.14 (0.05-0.34)   | 4          |
| IRAS 17208-0014 | ASCA      | 03/06/1996 | ...               | 3.0            | ...                | 2          |
| IRAS 20551-4250 | ASCA      | 10/19/1995 | ...               | 3.1            | ...                | 3          |
| IRAS 23128-5919 | ASCA      | 02/11/1995 | ...               | 3.4            | ...                | 3          |
| UGC 05101       | ASCA      | 11/17/1996 | 1.7               | 6.2            | ...                | 7          |
| NGC 6240        | ASCA      | 03/27/1994 | 6.4               | 19.            | 2.2                | 5          |
| NGC 6240        | BeppoSAX  | 08/15/1998 | 7.4               | 32.            | 1.6                | 6          |

REFERENCES. — 1. Iwasawa (1999); 2. Risaliti, Gilli, Maiolino, & Salvati (2000); 3. Misaki et al. (1999); 4. Severgnini et al. (2001); 5. Iwasawa & Comastri (1998); 6. Vignati et al. (1999); 7. This work

NOTE. — Fluxes in units of  $10^{-13}$  erg cm $^{-2}$  s $^{-1}$ .



TABLE 13. ULIRG PARAMETERS AND CLASSIFICATION

| Galaxy     | $L_{FIR}$<br>( $10^{12} L_{\odot}$ ) | $\frac{F_{25\mu m}}{F_{60\mu m}}$ | $\frac{F_{2-10 \text{ keV}}}{F_{FIR}}$<br>( $10^{-4}$ ) | Classification     |                                    | $\log N_{H,CO}^*$<br>( $\text{cm}^{-2}$ ) | $R_{CO}^{\dagger}$<br>(") | $R_{2-8 \text{ keV}}^{\ddagger}$<br>(") |
|------------|--------------------------------------|-----------------------------------|---|--------------------|------------------------------------|---|---------------------------|---|
|            |                                      |                                   |   | Optical            | IR                                 |   |                           |   |
| Arp 220    | 0.9                                  | 0.08                              | 0.27  | LINER <sup>1</sup> | HII <sup>2</sup>                   | 24.7                                      | 0.9                       | 0.9 (0.8-1.1)                           |
| IRAS 05189 | 0.7                                  | 0.25                              | 56  | S2 <sup>3</sup>    | AGN <sup>2</sup> , S1 <sup>4</sup> |   |                           | < 0.28                                  |
| IRAS 17208 | 1.6                                  | 0.05                              | 0.44  | HII <sup>1</sup>   | PDR <sup>5</sup>                   | 24.1                                      | 1.25                      | 1.0 (0.7-1.2)                           |
| IRAS 20551 | 0.6                                  | 0.15                              | 1.5   | HII <sup>6</sup>   | HII <sup>5</sup>                   |   |                           | < 0.70                                  |
| IRAS 23128 | 0.6                                  | 0.15                              | 4.8   | HII <sup>6</sup>   | HII <sup>5</sup>                   |   |                           | < 0.47                                  |
| Mkn 231    | 1.6                                  | 0.27                              | 8.6   | S1 <sup>3</sup>    | AGN <sup>2</sup>                   | 24.6                                      | 0.5                       | < 0.25                                  |
| Mkn 273    | 0.8                                  | 0.11                              | 5.8   | S2 <sup>1</sup>    | AGN <sup>2</sup>                   | >24.6                                     | < 0.6                     | < 0.47                                  |
| UGC 05101  | 0.6                                  | 0.09                              | 1.9   | LINER <sup>7</sup> | AGN <sup>8</sup> , SB <sup>9</sup> |   |                           | < 0.44                                  |
| NGC 6240   | 0.4                                  | 0.15                              | 17  | LINER <sup>7</sup> | SB <sup>9</sup>                    | 24.6                                      | 0.39                      | 1.1 (1.0-1.2)                           |

NOTE. —  $L_{FIR} = 2.58L_{60\mu m} + L_{100\mu m}$

\*Column density (in  $\text{cm}^{-2}$ ) inferred from the CO mass surface brightnesses given in Bryant & Scoville (1999).

<sup>†</sup>Deconvolved semimajor axis of CO emission given in Bryant & Scoville (1999).

<sup>‡</sup>Deconvolved semimajor axis of 2-10 keV emission, based on elliptical Gaussian fits (including PSF model) discussed in the text.

<sup>1</sup>Kim, Veilleux, & Sanders (1998)

<sup>2</sup>Imanishi & Dudley (2000)

<sup>3</sup>Veilleux, Kim, & Sanders (1999)

<sup>4</sup>Veilleux, Sanders, & Kim (1999)

<sup>5</sup>Laurent et al. (2000)

<sup>6</sup>Kewley, Heisler, Dopita, & Lumsden (2001)

<sup>7</sup>Veilleux, Kim, Sanders, Mazzarella, & Soifer (1995)

<sup>8</sup>Imanishi, Dudley & Maloney (2001)

<sup>9</sup>Lutz, Veilleux, & Genzel (1999)

hard X-ray spectrum of Mkn 231 appears to be genuinely flat ( $\Gamma < 1$ ).

In the Compton-thick scenario for an AGN origin to the hard X-rays, the hard X-ray would be due to some combination of reflection from optically-thick neutral material, scattering from optically-thin (and likely highly-ionized) material and leakage of X-rays through patches in the obscuring material. These effects would tend to flatten the observed X-ray spectrum and produce high-EW ( $> 1$  keV) Fe-K lines, as observed in samples of Seyfert 2 (Turner et al. 1997) and composite starburst-Seyfert (Levenson, Weaver, & Heckman 2001) galaxies (note that scattering from highly-ionized material alone would not flatten the observed X-ray spectrum). The fact that the hard X-ray emission tends to be coincident with CO gas with high implied column densities (see Table 13) supports this picture (although a caveat is discussed below), and this is clearly the case in NGC 6240. The Fe-K line EW in Mkn 273 is consistent with that expected to be produced by the transmission of X-rays through material with column densities of order  $10^{23}$  cm $^{-2}$  (Leahy & Creighton 1993), as is observed directly. However, there are insufficient counts in most of these spectra to allow meaningful constraints to be placed on complex models (i.e., involving reflection and “leaky” absorbers). Partial-covering fits to the XMM-Newton spectra of IRAS 05189-2524 and UGC 05101 and the Chandra spectrum of Mkn 231 (Gallagher et al. 2002) are in fact consistent with a highly-obscured hard X-ray source that is leaky or contains one or more scattering or reflection regions. Similar results based on XMM-Newton observations of ULIRGs are given in Braitto et al. (2002). Also note that if a highly-ionized scattering medium is acting as a mirror for the hard X-rays, then the Fe-K lines expected from such a mirror would be due to Fe XXV and Fe XXVI (K $\alpha$  energies of 6.7 and 6.9 keV) with EWs on the order of 0.5-1.0 keV (Bianchi & Matt 2002). We suggest that in these AGN ULIRGs the amounts of reflected and/or leaked flux and scattered flux are comparable to each other, effectively reducing the equivalent widths expected from neutral and ionized Fe-K to values within the range of our upper-limits. In the case of IRAS 05189-2524, the very tight constraint on neutral Fe-K suggests that the flux is mostly scattered and not reflected (or again IRAS 05189-2524 is simply Compton-thin).

Note that the long-term variability observed in the AGN ULIRGs implies that both the scattering and reflecting material must be located within 1-2 pc of the central X-ray sources, or distances consistent with the expected size the putative tori. However, this argues against the arcsecond-scale CO gas being a source of reflection that *dominates* the hard X-ray flux in the AGN ULIRGs. This is consistent with the relatively high  $L_{2-10\text{ keV}}/L_{IR}$  ratio of AGN ULIRGS, i.e., the molecular gas is most likely only directly obscuring the AGN with columns of order  $10^{23}$  cm $^{-2}$  or less. In general the CO gas appears to be distributed in 100-500 pc scale disks, and the disks are either viewed face-on and/or (particularly in the case of double nuclei) the nuclei are not located centrally in the disks (Bryant & Scoville 1999; Downes & Solomon 1998). Both of these effects would result in lower column densities being observed toward the nuclei than the peak values derived from the CO

data.

Turning to the starburst-ULIRGs, the hard X-ray emission is too weak for strong constraints to be placed on its spectral form (it is consistent with either a weak AGN viewed through modest columns, or a typical starburst). Moreover, the upper limits on the Fe K $\alpha$  EW are not restrictive. The extended hard X-ray emission resolved by Chandra in NGC 6240 suggests that starburst processes such as these may be contributing significantly (i.e., the two nuclei contribute  $< 50\%$  of the 2-10 X-ray flux of NGC 6240 although, as shown in Komossa et al. (2003), the nuclei dominate in the 5-8 keV band). These possibilities will be discussed in more detail in a subsequent paper.

### 6.3. The X-ray Emission of ULIRGs in Context

#### 6.3.1. The Far-Infrared

We have argued above that the signature of an AGN is possibly present in the hard X-ray emission of at least three of the eight ULIRGs in our sample (the same three that show evidence for an AGN in their optical and IR spectra), and that Fe-K emission shows that an energetically-important AGN is present in two of the starburst ULIRGs. One way to assess possible energetic contribution of AGN is to compare the ratio of the hard X-ray to far-infrared luminosities in the ULIRGs to values in typical AGN and starbursts.

Following Levenson, Weaver, & Heckman (2001, hereafter LWH), we first plot the ratio of hard X-ray to FIR luminosity as a function of the  $F_{25\mu\text{m}}/F_{60\mu\text{m}}$  flux ratio (Figure 5). The latter (a measure of luminosity-weighted mean dust temperature) is a useful empirical diagnostic to help assess the relative energetic importance of AGN and starburst activity in a galaxy (de Grijp, Miley, & Lub 1987). We compare the ULIRGs to a sample of starbursts observed by ASCA (Dahlem, Weaver & Heckman 1998; Della Ceca et al. 1996, 1999; Moran, Lehnert, & Helfand 1999; Ptak et al. 1999; Turner et al. 1997), a sample of composite starburst/Seyfert 2 galaxies, and the “pure” Seyfert 2 and Seyfert 1 galaxies samples from LWH. As shown by LWH, the pure Seyfert 2’s are generally Compton-thin and the composite starburst/Seyfert 2’s are generally Compton-thick. Since these other samples are based on ASCA data, the ULIRG 2-10 keV luminosities were taken from the global spectral fits, although we also plot the points derived from the nuclear fluxes for comparison. The IRAS infrared fluxes have been taken from NED, and starburst galaxies for which the global fluxes differ by more than 10% from the point-source values have been taken from Soifer et al. (1989).

Several results are clear from this comparison. First, both the mid/far-IR color and the relative strength of the hard X-ray continuum emission in the ULIRGs is generally similar to the values for starburst galaxies. The latter ratio is typically about two orders-of-magnitude below the values for most type 1 Seyferts and pure (Compton-thin) type 2 Seyfert galaxies. IRAS 05189-2524 is the only ULIRG lying outside the starburst regime and overlapping the pure type 2 Seyfert regime. Note that we are using observed hard X-ray luminosities in these plots, and correcting for the  $\sim 10^{23}$  cm $^{-2}$  column density in Mkn 273 would increase its 2-10 keV

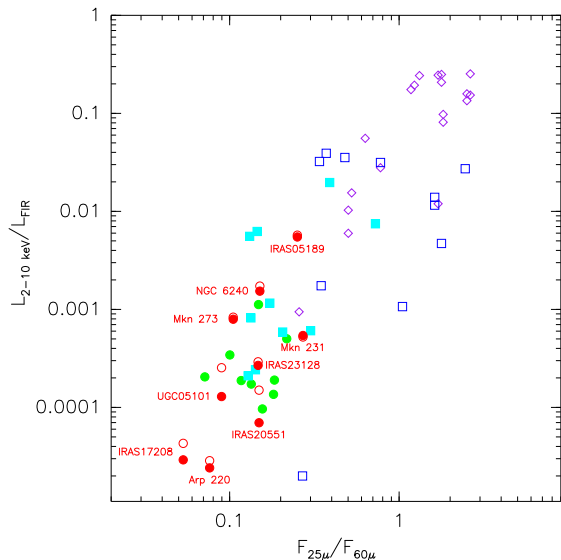


FIG. 5.—  $L_{2-10 \text{ keV}}/L_{\text{FIR}}$  vs.  $F_{25\mu}/F_{60\mu}$ . The plot key is: ULIRGS=red circles (values shown with filled circles are based on X-ray fluxes derived from the nuclear spectrum), starbursts = green filled circles, Seyfert 2s = blue squares, composites = cyan filled squares, Seyfert 1s = purple diamonds.

luminosity by a factor of  $\sim 3$  and place it in the HX/FIR  $> 10^{-3}$  Compton-thin regime. There is some overlap between the ULIRGs and the (Compton-thick) composite starburst/Seyfert 2 galaxies, but the ULIRGs as-a-class are even more extreme. Thus, in a purely empirical energetic sense there is a need to invoke a significant contribution of an AGN to the hard X-ray emission in only one of the eight ULIRGs. Second, the three AGN-ULIRGs (and NGC 6240) have significantly higher ratios of hard X-ray to far-IR luminosity than the starburst-ULIRGs. This suggests that in fact an AGN *is* contributing significantly to the hard X-ray emission in these former cases.

The above conclusions are reinforced by Figure 6, where we have plotted the ratio of Fe K $\alpha$  and far-IR luminosities *vs.* the ratio of hard X-ray and far-IR luminosities for the above samples of ULIRGs and AGN. In particular, the upper limits to the ratio of the Fe K $\alpha$  and far-IR fluxes in the ULIRGs lie below even the very low ratios observed in the Compton-thick starburst/Seyfert 2 composites, and are up to two orders-of-magnitude lower than in the pure type 2 Seyferts.

### 6.3.2. The [OIII] $\lambda 5007$ Line

The [OIII] $\lambda 5007$  emission-line is the strongest optical line produced in the kpc-scale Narrow Line Region, and is often used as a rough indicator of the true luminosity of the AGN in both type 1 and type 2 Seyferts. On this basis, Bassani et al. (1999) have proposed using the ratio of the hard X-ray and [OIII] $\lambda 5007$  fluxes as an indicator of X-ray absorption that is valid even in the Compton-thick regime. They also show that there is a strong inverse correlation between the hard X-ray/[OIII] flux ratio and the Fe K $\alpha$  equivalent width, with Compton-thick type 2 Seyfert nuclei at one extreme and type 1 Seyferts at the other.

In Figure 7 we plot the luminosities of the [OIII] $\lambda 5007$  lines *vs.* those of the Fe K $\alpha$  lines for Seyferts and ULIRGs. We have also corrected the [OIII] for dust

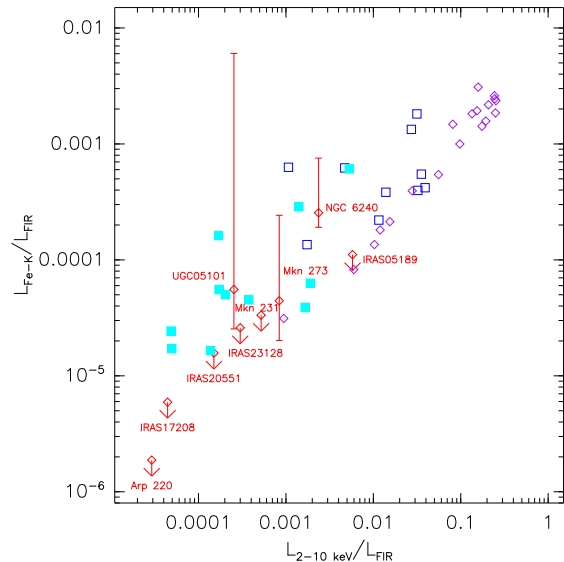


FIG. 6.—  $L_{2-10 \text{ keV}}/L_{\text{FIR}}$  vs.  $L_{\text{Fe-K}}/L_{\text{FIR}}$ . The upper-limits are based on fluxes listed in Table 6.

extinction using the prescription (based on the Balmer decrement) given in Dahari & De Roberts (1988). In the case of the ULIRGs we used the  $H\alpha/H\beta$  flux ratio listed in Table 14 while we applied mean corrections (also based on the statistical analysis in Dahari & De Roberts 1988) to the Seyfert 1 and Seyfert 2 samples (which increased the [OIII] fluxes by factors of 4 and 10, respectively). In the plot of the extinction-corrected [OIII] luminosity, the Seyferts exhibit a correlation with roughly unit slope and a scatter of  $\sim \pm 0.5$  dex. This suggests that both the Fe K $\alpha$  line and the [OIII] $\lambda 5007$  line can be used as very rough indicators of the luminosity of the hidden AGN, even in Compton-thick type 2 Seyferts. Since we have Fe K $\alpha$  detections for only two of the eight ULIRGs, we can only say that the data are consistent with the ULIRGs following the same trend as the Seyferts. More to the point, the relative weakness of the K $\alpha$  line in the ULIRGs (Figure 6) suggests that energetically dominant AGN are not present in most ULIRGs (even though AGN may contribute significantly to the hard X-ray emission in some cases).

To further assess the possible contribution of an AGN to the hard X-ray emission in ULIRGs, we have plotted the ratio of the hard X-ray and [OIII] $\lambda 5007$  flux (see Table 14) *vs.* the ratio of the hard X-ray and far-IR flux for our samples of ULIRGs and Seyferts (Figure 8). Prior to [OIII] extinction correction the ULIRGs occupy a distinct part of parameter space in this figure. On the one hand, they have ratios of hard X-ray to [OIII] flux that are most similar to type 1 and pure (Compton-thin) type 2 Seyfert galaxies, and are significantly larger than in the Compton-thick starburst/Seyfert 2 composites. Following Bassani et al. (1999), this implies only modest X-ray absorption in the ULIRGs. On the other hand (as discussed above) the ULIRGs have extremely small ratios of hard X-ray to far-infrared flux. After extinction-correcting the [OIII] fluxes, the ULIRGs better overlap the locus of the Compton-thick Seyfert 2 and composite galaxies, albeit with much more dispersion. The larger dispersion in the ULIRG sample is due at least in part to

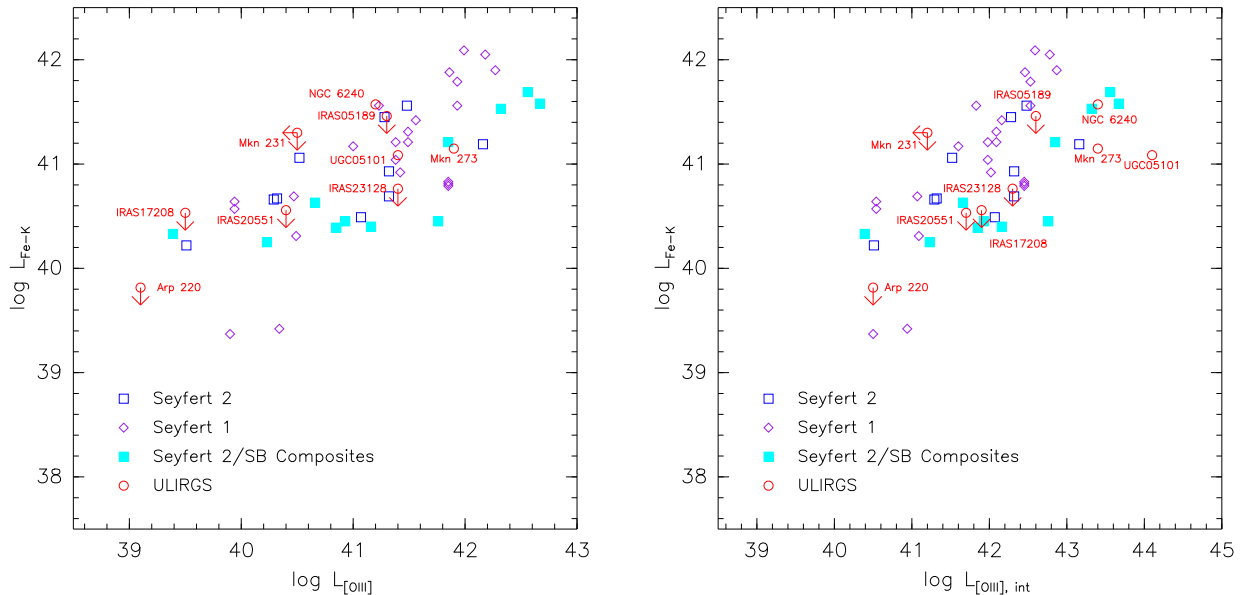


FIG. 7.— Fe-K luminosity plotted as a function of [OIII] line luminosity. (left) Plot generated using observed [OIII] luminosities; (right) plot generated using extinction-corrected [OIII] luminosities (see text). The plot key is: ULIRGS=red circles, Seyfert 2s = blue squares, composites = cyan filled squares, Seyfert 1s = purple diamonds.

the large (and hence uncertain) corrections to the [OIII] fluxes. Taking the extinction-corrected [OIII] fluxes at face-value, the AGN-ULIRGs Mkn 231 and IRAS 05189-2524 and the starburst-ULIRG Arp 220 have hard X-ray to [OIII] flux ratios similar to Compton-thin Seyferts, the AGN-ULIRG Mkn 273, the starburst-ULIRG UGC 05101, and NGC 6240 have ratios similar to Compton-thick Seyferts, and the starburst-ULIRGS IRAS 17208-0014, IRAS 20551-4250, and IRAS 23128-5919 are intermediate.

## 7. SUMMARY

We have presented the initial results from a Chandra survey of a complete sample of the 8 nearest ( $z \leq 0.04$ ) ultraluminous IR galaxies (ULIRGs) plus NGC 6240, using the hard X-rays (2-8 keV) to search for the possible presence of an obscured AGN, and to assess its contribution to the bolometric luminosity. In six cases (including NGC 6240), the extant optical and infrared spectra suggest that a starburst dominates the energetics (the "starburst-ULIRGs"), while an energetically significant AGN is present in the other three (the "AGN-ULIRGs"). We find that the hard X-ray properties of these two subtypes differ as well.

A hard X-ray source is detected in the nuclear region in every case. The nuclear source is spatially-resolved in two of the starburst-ULIRGs Arp 220 and IRAS 17208-0014 (FWHM  $\sim 1$  kpc and 4 kpc respectively) and also in NGC 6240, and is unresolved (FWHM  $\lesssim 0.5$  kpc) in the others. The upper limits to the spatial extent in the six unresolved cases are consistent with either an AGN or a compact starburst. Hard X-ray emission on larger (galactic) spatial scales is significant in six cases (all starburst-ULIRGs), comprising 10 to 50% of the total flux. We have shown that five starburst-ULIRGs have hard X-ray luminosities about an order-of-magnitude smaller than the three AGN-ULIRGs, with the hard X-ray luminosity of NGC 6240 being comparable to the AGN-ULIRGs.

Our analysis of the hard X-ray spectra provides no direct evidence for absorbing columns in excess of  $\sim 10^{23}$   $\text{cm}^{-2}$  except for in Mkn 273, although the data are relatively poor for the five starburst-ULIRGs. The Fe  $K\alpha$  line is convincingly detected in Mkn 273 and NGC 6240 and marginally detected in UGC 05101.

The ratio of the hard X-ray to far-IR flux in the ULIRGs (HX/FIR) is about three (two) orders of magnitude smaller than in type 1 (Compton-thin type 2) Seyfert galaxies. Only the AGN-ULIRG IRAS05189-2524 has a value for HX/FIR that is significantly higher than that in typical starburst galaxies, and only IRAS 05189-2524 and Mkn 231 are in the Compton-thin regime of a HX/FIR *vs.* HX/[OIII] plot. The three X-ray-brightest ULIRGS (the AGN-ULIRGs) and NGC 6240 have intermediate values of HX/FIR similar to the Seyfert 2/ starburst composite systems studied by LWH. Likewise, the flux ratio of the Fe  $K\alpha$  line and far-IR continuum is usually at least two orders-of-magnitude smaller in the ULIRGs than in typical Seyfert galaxies (but with some overlap with the Seyfert2/starburst composites). We show that type 1 and type 2 Seyferts follow a correlation between the [OIII] $\lambda 5007$  and Fe  $K\alpha$  luminosities. The weakness of the [OIII] and Fe  $K\alpha$  emission in the ULIRGs (relative to the far-IR) suggests a correspondingly weak AGN, although a highly-absorbed AGN (possibly) in conjunction with a complex scattering geometry cannot be ruled out.

Existing optical and IR spectroscopy show that AGN are definitely present in three of the ULIRGs, and we conclude that these AGN make a significant contribution to the observed hard X-ray emission in these cases. There is no compelling reason to invoke the presence of an AGN in the other five cases except for the strong Fe-K emission in UGC 05101 and NGC 6240 (where the AGN contribution to hard X-rays is also well established from the BeppoSAX PDS data; Vignati et al. 1999). Even in the three AGN-ULIRGs, the contribution of the AGN to the

TABLE 14. ULIRG [OIII] DATA

| Galaxy           | $L_{[OIII]}$<br>( $10^{40}$ ergs $s^{-1}$ ) | Reference | $L_{H\alpha}/L_{H\beta}$ | Reference |
|------------------|---|-----------|--------------------------|-----------|
| Arp 220          | 0.10  | 1         | 9.1                      | 1         |
| IRAS 05189-2524  | 62.   | 1         | 8.3                      | 1         |
| IRAS 17208-0014  | 3.7   | 2         | 18.6                     | 3         |
| IRAS 20551-4250  | 28.   | 4         | 9.6                      | 4         |
| IRAS 23128-5919* | 18.   | 4         | 7.0                      | 4         |
| Mkn 231          | < 3.2                                       | 5         | 5.4                      | 6         |
| Mkn 273          | 18.   | 7         | 10.                      | 3         |
| UGC 05101        | 1.6   | 8,9       | 23.4                     | 8         |
| NGC 6240         | 16.   | 10, 11    | 16.1                     | 8         |

REFERENCES. — 1. Veilleux, Kim, & Sanders (1999); 2. Kim, Veilleux, & Sanders (1998); 3. Veilleux, Sanders, & Kim (1999); 4. Duc, Mirabel, & Maza (1997); 5. unpublished data; 6. Dahari & De Roberts (1988); 7. Wittle (1992); 8. Veilleux, Kim, Sanders, Mazzarella, & Soifer (1995); 9. Kim, Veilleux, & Sanders (1995); 10. Armus, Heckman & Miley (1989); 11. Armus, Heckman & Miley (1990)

\*Values cited are for the southern nucleus of IRAS 23128-5919, which dominates the hard X-ray emission.

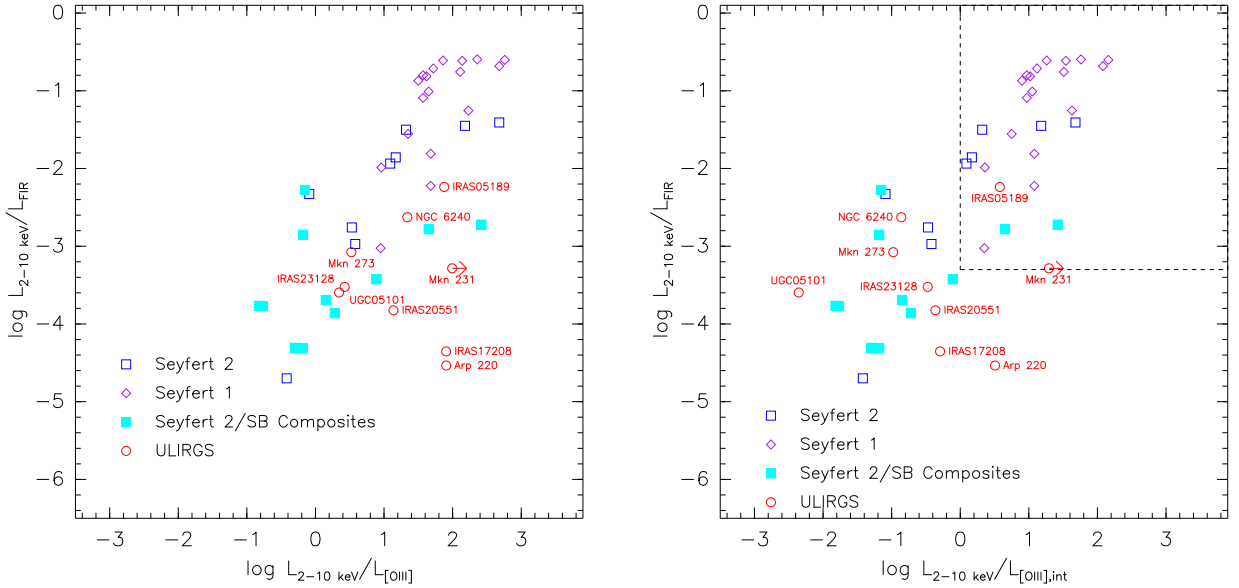


FIG. 8.— 2-10 keV/FIR luminosity plotted as a function of 2-10 keV/[OIII] luminosity. (left) Plot generated using observed [OIII] luminosities; (right) plot generated using extinction-corrected [OIII] luminosities (see text). The box delineated in the upper-right corner shows the region where Compton-thin Seyfert 2s are found in Panessa & Bassani (2002). The plot key is: ULIRGS=red circles, Seyfert 2s = blue squares, composites = cyan filled squares, Seyfert 1s = purple diamonds.

bolometric (IR) luminosity is quite uncertain. To make a major contribution, an AGN must be buried behind highly Compton-thick material with a very small transmitted or reflected fraction compared to typical Seyfert galaxies. This could be possible (given the very large column densities of molecular gas observed in the nuclei of these galaxies), but our new data provide no direct evidence for such high absorbing columns.

Of course, absence of evidence is not evidence of absence: it is exceedingly difficult to robustly prove that powerful AGN can not be present in these galaxies. However, we conclude that our new data provide no evidence that powerful “buried quasars” dominate the overall en-

ergetics of most ULIRGs, particularly those with a starburst optical or IR classification.

We would like to thank the anonymous referee for useful comments. This work made use of the NASA Extragalactic Database (NED), the NASA High-Energy Astrophysics Science and Research Center (HEASARC), the NASA Astrophysics Data System Bibliographic Services, and the Chandra X-ray Center Chandra Data Archive. This work was supported by the NASA grants NAG5 9910 and GO1-2086X.

#### REFERENCES

Armus, L., Heckman, T., & Miley, G. 1989, *ApJ*, 347, 727  
 Armus, L., Heckman, T., & Miley, G. 1990, *ApJ*, 364, 471

Arribas, S., Colina, L., & Clements, D. 2001, *ApJ*, 560, 160  
 Bassani, L. et al. 1999, *ApJS*, 121, 473

- Bianchi, S. & Matt, G. 2002, *ã*, 387, 76
- Blain, A., Smail, I., Ivison, R., & Kneib, J.-P. 1999, *MNRAS*, 302, 632
- Braito, V. et al. 2002, Proc. Symposium “New Visions of the X-ray Universe in the XMM-Newton and Chandra Era”, astro-ph/0202352
- Bryant, P. & Scoville, N. 1999, *ApJ*, 117, 2632
- Cappi, M. et al. 1999, *ã*, 350, 777
- Cash, W. 1979, *ApJ*, 228, 939
- Clements, D., Sutherland, W., McMahon, R. & Saunders, W. 1996, *MNRAS*, 279, 477
- Clements, D. et al. 2002, *ApJ*, 581, 974
- Condon, J., Huang, Z., Yin, Q., & Thuan, T. 1991, *ApJ*, 65
- Condon, J., Helou, G., Sanders, D., & Soifer, B. 1996, *ApJS*, 103, 81
- Dahari, O. & De Roberts, M. 1988, *ApJS*, 67, 249
- Dahlem, M., Weaver, K. & Heckman, T. 1998, *ApJS*, 118, 401
- Davis, J. 2001, *ApJ*, 562, 575
- de Grijp, M., Miley, G., & Lub, J. 1987, *A&AS*, 70, 95
- Duc, P.-A., Mirabel, I. & Maza, J. 1997, *A&A*, 124, 533
- Della Ceca, R., Griffiths, R., Heckman, T., & MacKenty, J. 1996, *ApJ*, 469, 662
- Della Ceca, R., Griffiths, R., Heckman, T., Lehnert, M., & Weaver, K. 1999, *ApJ*, 514, 772
- Dickey, J. & Lockman, F. 1990, *Ann. Rev. Ast. Astr.* 28, 215
- Downes, D. & Solomon, P. 1998, *ApJ*, 507, 615
- Eracleous, M., Shields, J., Chartas, G., & Moran, E. 2002, *ApJ*, 565, 108
- Ferrarese, L. & Merritt, D. 2000, *ApJ*, 539, L9
- Gallagher, S., Brandt, W., Chartas, G., Garmire, G., & Sambruna, R. 2002, *ApJ*, 569, 655
- Genzel, R., Lutz, D., Sturm, E., Egami, E., Kunze, D., Moorwood, A., Rigopoulou, D., Spoon, H., Sternberg, A., Tacconi-Garman, L., Tacconi, L., & Thatte, N. 1998, *ApJ*, 498, 579
- Genzel, R., Tacconi, L., Rigopoulou, D., Lutz, D., & Tecza, M. 2001, *ApJ*, 563, 527
- Griffiths, R., et al. 2000, *Science*, 290, 1325
- Grimm, H., Gilfanov, M., & Sunyaev, R. 2003, *MNRAS*, 339, 793
- Imanishi, M. & Dudley, C. 2000, *ApJ*, 545, 701
- Imanishi, M., Dudley, C., & Maloney, P. 2001, *ApJ*, 558, 93
- Iwasawa, K. & Comastri, A. 1998, *MNRAS*, 297, 1219
- Iwasawa, K. 1999, *MNRAS*, 302, 96
- Joseph, R. 1999, *Ap&SS*, 266, 321
- Kewley, L., Heisler, C., Dopita, M., & Lumsden, S. 2001, *ApJS*, 132, 37
- Kim, D.-C., Veilleux, S., & Sanders, D. 1998, *ApJS*, 98, 129
- Kim, D.-C., Veilleux, S., & Sanders, D. 1998, *ApJ*, 508, 627
- Kim, D.-C. & Sanders, D. 1998, *ApJS*, 119, 41
- Komossa, S., Burwitz, V., Hasinger, G., Predehl, P., Kaastra, J. S., & Ikebe, Y. 2003, *ApJ*, 582, L15
- Krolik, J. & Kallman, T. 1987, *ApJ*, 320, 5
- Laurent, O., Mirabel, I., Charmandaris, V., Gallais, P., Madden, M., Vigroux, L., & Cesarsky, C. 2000, *A&A*, 359, 887
- Levenson, N. A., Weaver, K., & Heckman, T. 2001, *ApJ*, 550, 230
- Levenson, N., Krolik, J., Zycki, P., Heckman, T., Weaver, K., Awaki, H., & Terashima, Y. 2002, *ApJ*, 573, 81L
- Leahy, D. & Creighton, J. 1993, *MNRAS*, 263, 314
- Liedahl, D.A., Osterheld, A.L., and Goldstein, W.H. 1995, *ApJL*, 438, 115
- Lira, P., Ward, M., Zezas, A., Alonso-Herrero, A., & Ueno, S. 2002, *MNRAS*, 330, 259
- Lira, P., Ward, M., Zezas, A. & Murray, S. 2002, *MNRAS*, 333, 709
- Lutz, D., Veilleux, S., & Genzel, R. 1999, *ApJ*, 517, 13
- Magdziarz, P. & Zdziarski, A. 1995, *MNRAS*, 273, 837
- Martin, C., Kobulnicky, H., & Heckman, T. 2002, *ApJ*, 574, 663
- McDowell, J. et al. 2003, *ApJ*, in press, astro-ph/0303316
- Misaki, K., Iwasawa, K., Taniguchi, Y., Terashima, Y., Kunieda, H., Watarai, H. 1999, *Adv. Sp. Research*, 23, 1051
- Moran, E., Lehnert, M., & Helfand, D. 1999, *ApJ*, 526, 649
- Mushtozky, R., Done, C., & Pounds, K. 1993, *ARA&A*, 31, 717
- Norman, C. & Scoville, N. 1988, *ApJ*, 332, 124
- Norris, R. 1988, *MNRAS*, 230, 345
- Panessa, E. & Bassani, L. 2002, *ã*, 394, 435
- Persic, M., & Rephaeli, Y. 2002, *ã*, 382, 843
- Planesas, P., Mirabel, I., & Sanders, D. 1991, *ApJ*, 370, 172
- Ptak, A., Yaqoob, T., Serlemitsos, P. J., Kunieda, H., & Terashima, Y. 1996, *ApJ*, 459, 542
- Ptak, A., Serlemitsos, P., Yaqoob, T., Mushotzky, R. 1999, *ApJS*, 120, 179
- Ptak, A. & Griffiths, R. 1999, *ApJ*, 517, 85
- Ptak, A. & Griffiths, R. 2002, *Astronomical Data Analysis Software and Systems XII*, ASP Conference Proceedings Series, in press., astro-ph/0303104
- Risaliti, G., Gilli, R., Maiolino, R. & Salvati, M. 2000, *A&A*, 357, 13
- Rothernflug, R. & Arnaud, M. 1985, *A&A*, 144, 431
- Sanders, D. & Mirabel, I. 1996, *ARA&A*, 34, 749
- Sanders, D. 1999, *Ap&SS*, 266, 331
- Scoville, N., Sargent, A., Sanders, D., & Soifer, B. 1991, *ApJ*, 366, 5
- Severini, P., Risaliti, G., Marconi, R., & Salvati, M. 2001, *A&A*, 368, 44
- Soifer, B., Boehmer, G., Neugebauer, G., & Sanders, D. 1989, *AJ*, 98, 766
- Strickland, D., Heckman, T., Weaver, K., Hoopes, C., & Dahlem, M. 2002, *ApJ*, 568, 689
- Taniguchi, Y., Yoshino, A., Ohya, Y., & Nishiura, S. 1999, *ApJ*, 514, 660
- Terashima, Y., Iyomoto, N., Ho, L., & Ptak, A. 2002, *ApJS*, 139, 1
- Terashima, Y., Ho, L., & Ptak, A. 2000, *ApJ*, 539, 161
- Thean, A., Pedlar, A., Kukula, M., Baum, S. & O’Dea, C. 2000, *MNRAS*, 314, 573
- Tremaine, S., Gebhardt, K., Bender, R., Bower, G., Dressler, A., Faber, S., Filippenko, A., Green, R., Grillmair, C., Ho, L., Kormendy, J., Lauer, T., Magorrian, J., Pinkney, J., & Richstone, D. 2002, *ApJ*, 574, 740
- Turner, T., George, I., Nandra, K., & Mushotzky, R. 1997, *ApJS*, 113, 23
- Yun, M. & Scovilla, N. 1995, *ApJ*, 451, L45
- Veilleux, S., Kim, D.-C., Sanders, D., Mazzarella, J., & Soiffer, B. 1995, *ApJS*, 98, 171
- Veilleux, S., Kim, D.-C., & Sanders, D. 1999, *ApJ*, 522, 113
- Veilleux, S., Sanders, D., & Kim, D.-C. 1999, *ApJ*, 522, 139
- Vignati, P. et al. 1999, *ã*, 349, L57
- Weaver, K., Heckman, T. & Dahlem, M. 2000, *ApJ*, 534, 684
- Weaver, K., Heckman, T., Strickland, D., & Dahlem, M. 2002, *ApJ*, 576, 19L
- Wittle, M. 1992, *ApJS*, 79, 49
- Xia, X., Xue, S., Mao, S., Boller, T., Deng, Z., & Wu, H. 2002, *ApJ*, 564, 196
- Zeas, A. & Fabbiano, G. 2002, *ApJ*, 577, 726